

Report No. _____

CSA-76-8085-3

Contract No. _____

DAAB07-76-C-8085



12
LEVEL



EXECUTIVE SUMMARY

ADAPTIVE ANTENNA CONTROL (AAC) PROGRAM

March 1981

Dr. P. Monsen
Dr. S.A. Parl

SIGNATRON, Inc.
12 Hartwell Avenue
Lexington, Massachusetts 02173



DTIC FILE COPY

DISTRIBUTION STATEMENT

Approved for public release;
distribution unlimited.

**U. S. ARMY
COMMUNICATIONS SYSTEMS AGENCY
Fort Monmouth, New Jersey**

MONITORING OFFICE
U. S. ARMY
COMMUNICATIONS R&D COMMAND
Fort Monmouth, NJ

818 13008

AD A103385

The views, opinions, and/or findings contained in this report are those of the author(s) and should not be construed as an official Department of the Army position policy, or decision unless designated by other documentation.

UNCLASSIFIED

SECURITY CLASSIFICATION OF THIS PAGE (When Data Entered)

11 JUN 81

17 REPORT DOCUMENTATION PAGE

READ INSTRUCTIONS
BEFORE COMPLETING FORM

1. REPORT NUMBER 18/CSA 76-8085-7	2. GOVT ACCESSION NO. AD-A103385	3. RECIPIENT'S CATALOG NUMBER
4. TITLE (and Subtitle) 6. Adaptive Antenna Control (AAC) Program Revision A	5. TYPE OF REPORT & PERIOD COVERED Executive Summary	
7. AUTHOR Dr. Peter Monsen Dr. Steen Parl A	8. CONTRACT OR GRANT NUMBER(s) DAAB07-76-C-8085	
9. PERFORMING ORGANIZATION NAME AND ADDRESS SIGNATRON, INC. 12 Hartwell Avenue Lexington, MA 02173	10. PROGRAM ELEMENT, PROJECT, TASK AREA & WORK UNIT NUMBERS 1X763707D2451702	
11. CONTROLLING OFFICE NAME AND ADDRESS U.S. Army Communications Systems Agency Fort Monmouth, New Jersey	12. REPORT DATE 24 March 1981 Revision-June 1981	
14. MONITORING AGENCY NAME & ADDRESS (if different from Controlling Office) U.S. Army Communications Electronics Command Fort Monmouth, New Jersey Attn: DRSEL-COM-RM-2 12 61	13. NUMBER OF PAGES 54	
16. DISTRIBUTION STATEMENT (of this Report) Approved for public release; distribution unlimited.	15. SECURITY CLASS. (of this report) UNCLASSIFIED 17	
17. DISTRIBUTION STATEMENT (of the abstract entered in Block 20, if different from Report)		
18. SUPPLEMENTARY NOTES Notes		
19. KEY WORDS (Continue on reverse side if necessary and identify by block number) Angle Diversity Troposcatter Path Loss Prediction Decision Feedback Equalizer Digital Troposcatter Communication Coupling Loss Antenna		
20. ABSTRACT (Continue on reverse side if necessary and identify by block number) A theoretical and empirical investigation of angle diversity for application on Defense Communications System (DCS) tropospheric scatter communication links has been completed. This report summarizes the principal areas of this investigation. The major results are: (continued on reverse side)		

UNCLASSIFIED

SECURITY CLASSIFICATION OF THIS PAGE(When Data Entered)

20. (continued)

- (1) Development of a new propagation prediction model applicable at frequencies up to 5 GHz.
- (2) Development of a modem prediction model for calculating the bit error rate and fade outage on a fading multipath channel for the MD-918/GRC modem.
- (3) A trade-off analysis to determine the optimum angle diversity system.
- (4) Design and development of a 4.4 - 5.0 GHz (C-Band) angle diversity feedhorn which gives a beam separation within about 1/2 dB of optimum.
- (5) Theoretical and empirical evidence that angle diversity has a performance advantage over frequency diversity.
- (6) Discovery of reduced correlation effects in angle diversity when wideband signals are employed.
- (7) Development of a methodology and a statistical base for development of future angle diversity systems.

This effort impacts the development of future digital tropo-scatter circuits by establishing a new technology which will allow conversion from frequency to angle diversity with a resulting halving of frequency requirements and a positive system gain in almost all applications. The angle and frequency diversity systems have virtually the same level of complexity.

UNCLASSIFIED

SECURITY CLASSIFICATION OF THIS PAGE(When Data Entered)

FOREWORD

U.S. Army contract DAAB07-76-C-8085 to SIGNATRON, Lexington, MA sponsored a troposcatter radio investigation with application to Defense Communications System links over the time period from June 1976 to March 1980. The results of this investigation will be applied in the future digital conversion of DCS troposcatter links. The detailed technical developments, results, and conclusions have been presented in the Test Report (ADA 04416) and the Final Report (ADA 091764). This Executive Summary presents the major findings and results from this investigation.

Accession For	
NTIS GRA&I	<input checked="" type="checkbox"/>
DTIC TAB	<input type="checkbox"/>
Unannounced	<input type="checkbox"/>
Justification	
By	
Distribution/	
Availability Codes	
Dist	Avail and/or Special
A	

TABLE OF CONTENTS

<u>SECTION</u>		<u>PAGE</u>
1	INTRODUCTION.....	1
1.1	BACKGROUND.....	1
1.2	PROGRAM SUMMARY.....	2
1.3	REPORT OUTLINE.....	3
2	ANGLE DIVERSITY DESIGN.....	4
2.1	SYSTEM CONFIGURATION, FREQUENCY VS. ANGLE DIVERSITY.....	4
2.2	DIGITAL TRANSMISSION, A MODEM MODEL.....	7
2.3	BEAM CORRELATION AND SQUINT LOSS.....	15
2.4	ANTENNA POINTING ANGLE.....	21
3	TROPOSCATTER PATH PREDICTION TECHNIQUE.....	25
3.1	BACKGROUND.....	25
3.2	PROPAGATION MODEL SUMMARY.....	26
3.3	LONG TERM VARIABILITY.....	30
3.3.1	NBS Long Term Variability Model.....	32
3.3.2	Long Term Variability in a Angle Diversity System.....	34
4	PREDICTED AND MEASURED RESULTS.....	36
4.1	TROPOSCATTER LINK RESULTS.....	36
4.2	DIGITAL MODEM RESULTS.....	42
5	CONCLUSIONS	49

LIST OF FIGURES

Figure 1	2S/2F Configuration.....	5
Figure 2	2S/2A Configuration.....	6
Figure 3	Serial Data Transmission, Radio System.....	10
Figure 4	Decision-Feedback Equalizer, 4PSK.....	11
Figure 5	Uncorrelated Diversity Equivalent System.....	14
Figure 6	Troposcatter Path Structure.....	17
Figure 7	Outage Rate for C-band Link.....	19
Figure 8	Outage Rate for L-band Link.....	20
Figure 9	Correlation Loss, C-band Link.....	22
Figure 10	Predicted Outage Probability, RADC Link.....	37
Figure 11	Predicted Outage Probability, Sahin Tepari-Yamanlar Link.....	38
Figure 12	Probability RSL Exceeds Ordinate.....	42
Figure 13	Squint Loss Distributions.....	43
Figure 14	Multipath Spreads and Relative Delay Space/Angle Pair 1/5.....	44
Figure 15	2S/2F vs. 2S/2F/2A, Plotted Against Main Beam SNR.....	46
Figure 16	Quad Diversity Configurations Plotted Against Main Beam Path Loss.....	47

LIST OF TABLES

Table 1	Test Link Squint Angles.....	21
Table 2	Path Parameters.....	39
Table 3	Field Test Results, Predicted and Measured.....	40

SECTION 1
INTRODUCTION

1.1 BACKGROUND

Radio communication over distances beyond line-of-sight can be accomplished via a scattering mechanism which occurs in the troposphere. Most applications of this technique occur in the frequency range from 0.5 to 5.0 GHz. Achievable digital transmission capacities are on the order of 10^7 bits/second. Fundamental limitations to this capacity are transmission path loss and allocated bandwidth requirements. The scattering mechanism results in a time varying received signal with fluctuations on the order of 1Hz and a multipath smeared response over a delay range of a few hundred nanoseconds. The effects can be compensated for by the provision of redundant diversity channels and adaptive signal processing which can track the channel fluctuations and correct for multipath smearing. Some of the diversity techniques employed include space diversity which is achieved with multiple antennas, frequency diversity, polarization diversity which utilizes multiple antennas with polarization marking, and angle diversity. Angle diversity is achieved by using a multiple feedhorn structure in a parabolic reflector antenna to intercept more than one arriving signal. These diversity techniques are termed explicit diversity because they are explicitly designed as redundant channel paths for fading protection. The channel multipath also provides a diversity capability which can be exploited by adaptive signal processing techniques in a digital transmission system. This diversity form is denoted as implicit diversity.

Most present troposcatter systems use either a combination of space and frequency diversity or space and polarization diversity. These diversity configurations require two space diversity antennas and two transmit power amplifiers at each terminal. Frequency diversity has the disadvantage that it doubles the bandwidth allocation requirements. Polarization diversity may exhibit high correlation between diversity branches which in turn reduces the fading protection. The future conversions of old analog troposcatter systems to digital troposcatter systems has spurred interest in angle diversity as an alternative to either frequency or polarization channels.

Angle diversity in a troposcatter application has been extensively studied and reported on in the literature [1-9]. The findings of these reports could be summarized as

- for typical narrowbeam antennas, vertically displaced feeds provide less correlation between angle diversity channels than horizontally displaced feeds.
- the elevated diversity beam has a larger multipath delay spread also due to the larger scattering angle. The delay difference between the elevated and main beam was also found to vary and could not be completely compensated for with a fixed delay.
- the elevated diversity beam has a larger scattering angle and on the average has a larger path loss. This additional "squint loss" reduces the effectiveness of the diversity combining by approximately one-half the squint loss in dB due to the performance dependence on the geometric mean of the signal-to-noise ratios of the diversity branches.

The squint loss effect, correlation between diversity beams, larger multipath in the elevated beam, and delay variations between the beams generally led communicators to the conclusion that angle diversity was inferior in performance to frequency diversity. The investigation summarized in this report established that this conclusion was incorrect. Both the theoretical and experimental results from this investigation show that in a digital system application, angle diversity has generally equal or better performance than frequency diversity. Moreover, the system complexity of the angle diversity system is about the same as the frequency diversity system. Since angle diversity requires half the bandwidth of a frequency diversity system, these results mean that existing frequency diversity systems can be converted to angle diversity system with a performance improvement and either a capacity increase of 2 to 1 or a reduction in the number of bandwidth allocations by a factor of 2. The severe frequency congestion problem in the microwave frequency range can then be significantly alleviated by angle diversity applications.

1.2 PROGRAM SUMMARY

The effort described in this report consisted of three phases: the study phase, the equipment development phase and the link test. In brief, these phases consisted of the following:

- Study Phase: comprehensive models of the troposcatter propagation and digital modem characteristics were modeled. The propagation model emphasized the turbulent scatter mechanism as the limiting mode, particularly for S and C band (2.0-5.0 GHz) transmissions. This model was written in terms of spectrum slope, refractive index variance, and scale of turbulence. In the past, aperture-to-medium coupling loss has been included in total path loss calculations as a separate parameter, i.e., the total path loss is the basic path loss with omnidirectional antennas, the antenna gains, and the coupling loss. The usefulness of this concept is questionable, since it uses properties of the atmospheric structure outside the actual antenna beams. The approach developed in this study calculated the total path loss directly by integrating over the common volume. The digital modem model was developed to predict bit error rate (BER) statistics for the MD-918 troposcatter modem. This modem employs a decision-feedback equalizer as the means of combining diversity channels and minimizing intersymbol interference effects. The MD-918 modem has been tested in DCS troposcatter configurations in both the United States and in Europe. The propagation and digital modem models were used to predict the performance of angle diversity in replacing space or frequency diversity and in augmenting either or both for systems providing up to eighth order diversity.

- Equipment Development Phase: The angle diversity design was selected as a vertical splay of two beams spaced by approximately 1 beamwidth. A C-Band angle diversity feedhorn was developed with capability of duplex operation with up to 10 Kw transmitters and with dual polarization ports in both horn branches. A digital traffic capability was realized through the use of MD-918 digital tropo modems. A predetection combiner (PDC) was developed to implement up to 8th order diversity with the MD-918 for combining the signals of the elevated (i.e., the angle diversity) beams.

- Link Test Phase: The test program consisted of an extensive series of propagation and modem performance tests from October 1977 to May 1978 followed by an effort to collect long term propagation data. This second effort continued until October 1979. The test bed for these experiments was the RADC 168 mile C-Band troposcatter system between Youngstown and Verona, NY. Specific parameters measured were hourly path loss distributions, long term distributions of hourly median path loss, multipath profiles and rms multipath spread, short term correlation between angle diversity paths, long term decorrelation of angle diversity hourly medians, angle diversity squint loss statistics, and BER statistics at 6.3 and 12.6 Mb/s.

1.3 REPORT OUTLINE

This report summarizes the major findings of this investigation. In Section 2, we present the features in an angle diversity design for a digital transmission system. A new propagation model applicable up to 5GHz was developed for this study and is presented in Section 3. This section also includes an evaluation of long term variability in an angle diversity system. In Section 4 the major results of our analysis and field tests are presented. The major conclusions from this investigation are given in Section 5.

SECTION 2
ANGLE DIVERSITY DESIGN

2.1 SYSTEM CONFIGURATION, FREQUENCY VS. ANGLE DIVERSITY

Conventional troposcatter systems use two antennas per terminal and two bandwidth allocations per direction to achieve dual space/dual frequency (2S/2F) diversity. Angle diversity provides redundant paths by collecting different angle of arrival signals at the receiver. A dual angle diversity system, for example, would employ a two horn primary feed at the parabolic reflector focus instead of the conventional one horn primary feed. In the frequency diversity system, a power amplifier is required at each of the two RF carriers. To convert from dual frequency to dual angle, the second power amplifier is tuned to the same frequency as the first and a new feed structure is provided. The resulting dual space/dual angle (2S/2A) system now requires only one bandwidth allocation in each direction. Conversion to angle diversity halves the frequency requirements of present 2S/2F quadruple diversity systems. Since both diversity configurations have 4 diversity outputs, the systems are identical from the input to the receivers down through the modem to the data output. Figures 1 and 2 illustrate the 2S/2F and 2S/2A configurations. The 2S/2A system does not require a diplexer as does the 2S/2F system, but an additional waveguide run is needed from the feedhorn to the receivers. The 2S/2F system requires transmitters tuned to two frequencies, a single horn feed, and diplexers to separate the frequencies. The 2S/2A system has both transmitters tuned to the same frequency and a dual horn feed. The receivers and modem are identical in both configurations. The second transmitter in the 2S/2A configuration is required for redundancy in case of failure. Its on-the-air use provides 3dB more scattered power per diversity which tends to offset the squint loss from the elevated beam in the dual angle diversity structure. Previous to this investigation this engineering factor was not considered in a comparison of frequency and angle diversity.

This savings in bandwidth through use of angle diversity is potentially present with analog troposcatter systems, but it is largely dissipated by the more difficult implementation disadvantages of analog angle diversity. In an analog system, the time delay variation between the main and elevated beam and the additional multipath spread of the elevated beam are serious problems.

DUAL SPACE/DUAL FREQUENCY (2S/2F)
 QUADRUPLE DIVERSITY TROPOSCATTER TERMINAL

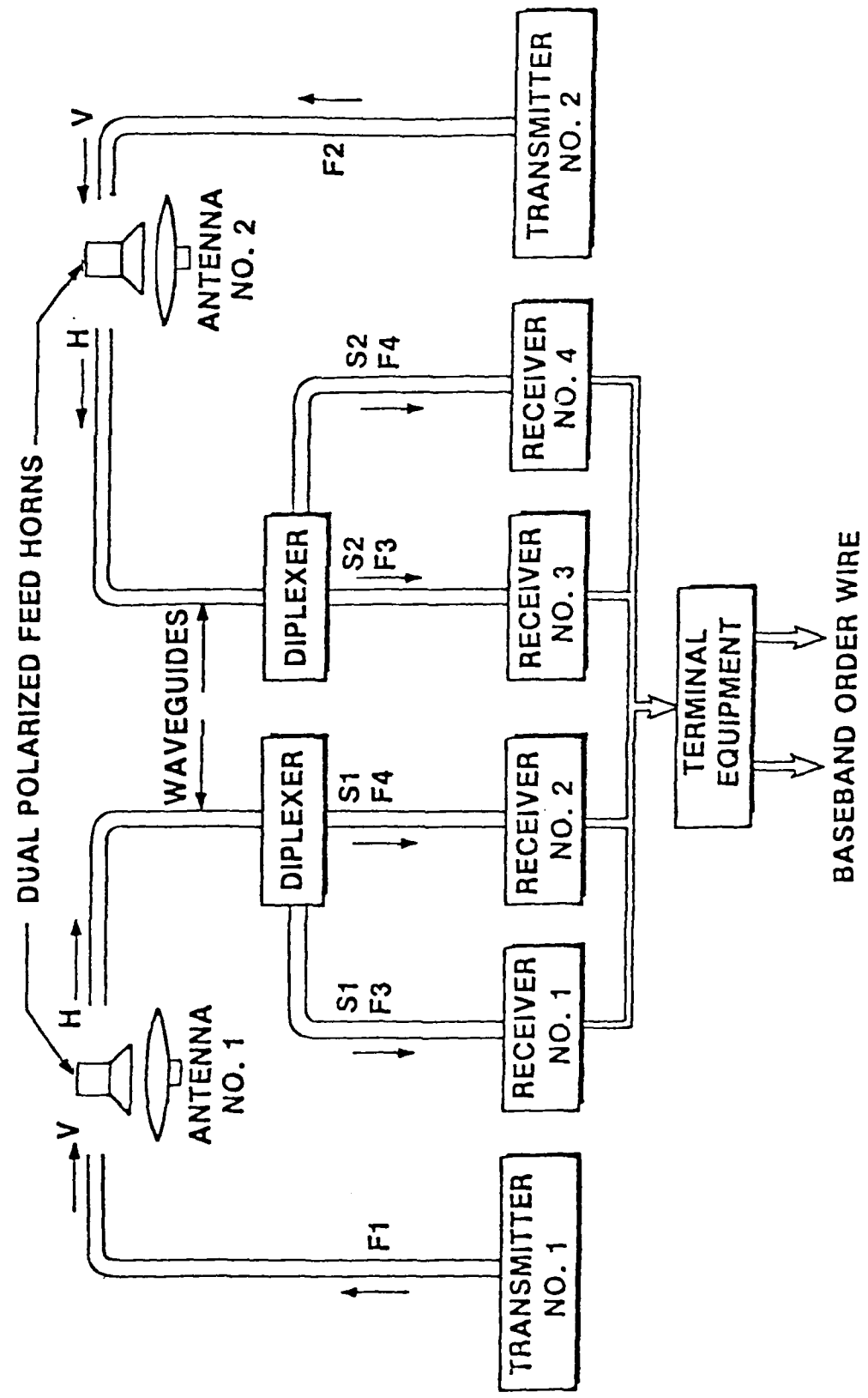


Figure 1 2S/2F CONFIGURATION

DUAL SPACE/DUAL ANGLE (2S/2A)
QUADRUPLE DIVERSITY TROPOSCATTER TERMINAL

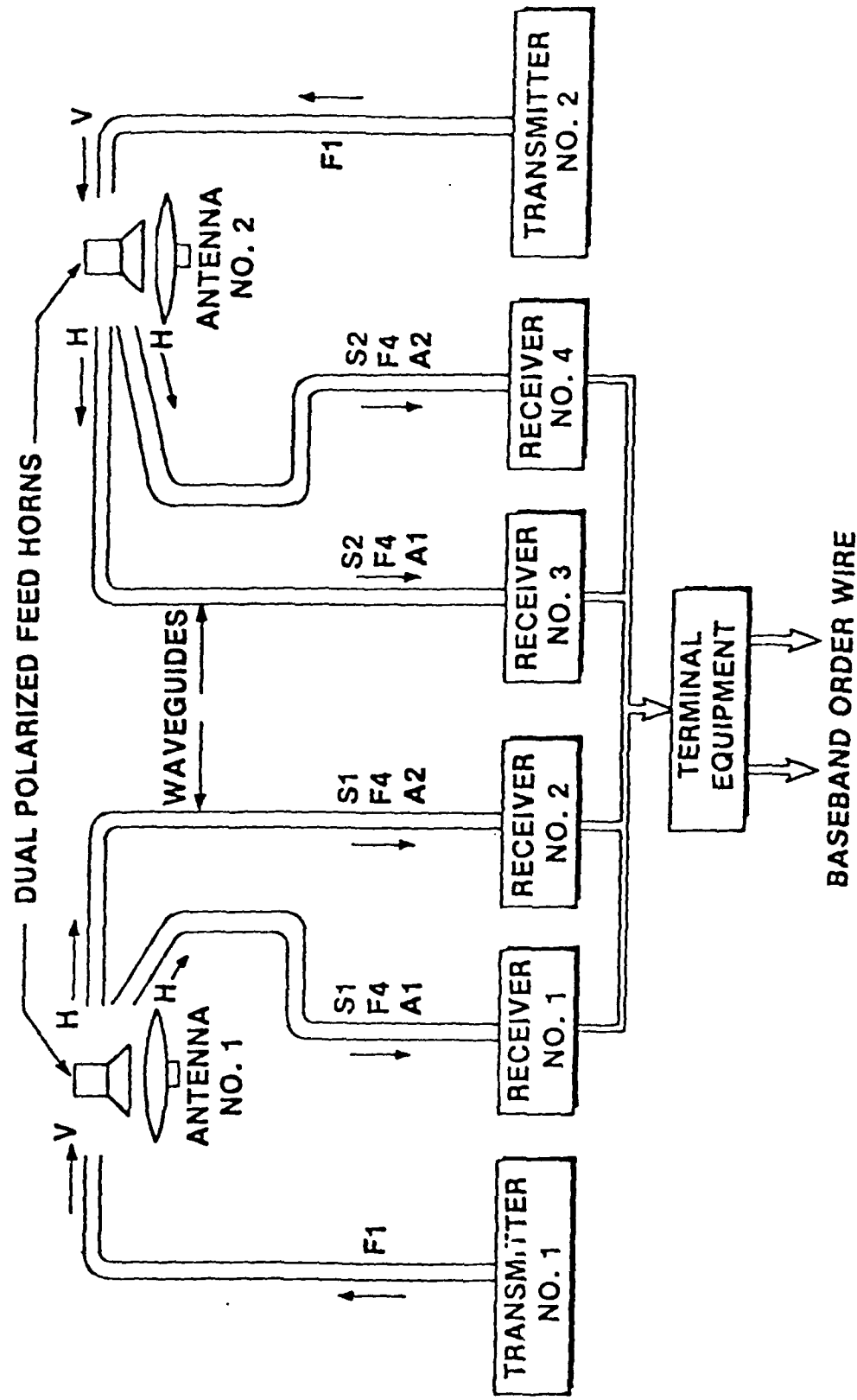


Figure 2 2S/2A CONFIGURATION

Adaptive processor techniques can compensate for these effects in a digital system.

2.2 DIGITAL TRANSMISSION, A MODEM MODEL

This study emphasized the use of a Decision-Feedback Equalizer (DFE) in a digital transmission angle diversity application. An adaptive DFE modem [10,11] using an equalizer input for each diversity branch operates to combine the diversity channels, mitigate the deleterious effect of intersymbol interference and to coherently collect the multipath energy thereby generating additional diversity. The tapped delay line filter structure in the equalizer also adaptively compensates for delay variations between signals arriving in the main and squinted angle diversity beam. This modem technique has been shown [12] in laboratory simulation and field tests to support rates up to 12 Mb/s on troposcatter diversity channels. The angle diversity design and optimization has been predicated on the use of an adaptive equalizer modem. We briefly outline here the performance model used to describe the DFE modem. Results from this model will be used subsequently to evaluate the angle diversity system and to compare predicted and measured performance. The performance model is an extension of the model first developed in [12] and is described in greater detail in the final report [13] on this program.

Performance of a digital troposcatter system can be expressed in terms of average bit error rate and outage probability. Although the average BER can be a useful parameter and is frequently measured in experimental tests, it lacks a direct relation of digitized voice quality in a troposcatter application. The outage probability is a measure of the fraction of time a fixed BER threshold is exceeded, i.e., the fraction of time the system is "out". The outage probability represents one point on the cumulative BER distribution function. Defense Communication System (DCS) standards for digital links are expressed in terms of a 7.5×10^{-4} yearly outage probability with a BER threshold criterion of 10^{-4} , since this level corresponds to the start of degraded digitized voice performance in a PCM system. For this reason the digital modem performance model will develop prediction of both average BER and outage probability.

The bit error rate performance of a digital data system operating over an angle diversity troposcatter link is dependent on the received power at each feedhorn, the correlation between diversity channels, and the multipath characteristics of the composite diversity system. We have developed a mathematical model to predict (1) the bit error rate statistics as a function of the hourly median received power for each diversity channel and (2) the long term probability that the bit error rate is exceeded. Statistics for the first prediction are based on the short term (less than a minute) fading characteristics of the troposcatter channel. The long term calculation deals with the availability of the digital troposcatter system as a result of hourly and daily variations in path parameters. Long term variability will be discussed separately in Section 3.

We present here the basic equations for the modem performance model in a non-diversity application and extend the result to include angle, frequency, or space diversity. The remainder of this subsection is provided for readers interested in the mathematical modeling approach for the DFE modem. Other readers may omit this portion and proceed to subsection 2.3. The performance of the DFE on a fading channel is a function of the radio/modem filters, the multipath profile of the channel, and the additive noise statistics. We consider a radio system as depicted in Figure 3. Here a modulator is used to convert a series of information digits to a continuous waveform $s(t)$. For purposes of analysis we consider 4PSK because of its spectral and detection efficiency. In complex notation the modulating waveform for a $2/T$ bit rate is

$$s(t) = \sum_{k=-\infty}^{\infty} s_k f(t-kT), \{s_k\} = \{\pm 1 \pm j\} . \quad (1)$$

Transmit and receive filters are defined with impulse responses $f_1(t)$ and $f_2(t)$, respectively. The combined filter response is defined as

$$f(t) = \int_0^{\infty} f_1(\tau) f_2(t-\tau) d\tau . \quad (2)$$

A continuous echo model of the troposcatter channel is used so the multipath profile $Q(\tau)$ represents the average received energy at a particular delay τ for impulse function excitation of the channel. The channel impulse response is taken as a complex Gaussian function in this model. One can show that the average received energy per bit is

$$\bar{E}_b = \int_0^{\infty} f_1^2(t) dt \int_0^{\infty} Q(\tau) d\tau . \quad (3)$$

We consider additive white Gaussian noise with spectral density N_0 Watts/Hz. The mean signal-to-noise ratio for this system is defined as

$$\bar{\rho} = \bar{E}_b / N_0 . \quad (4)$$

The demodulator in the system diagram of Figure 3 converts the RF signal into a baseband signal for processing by the equalizer and eventual symbol detection. The autocorrelation function of the noise process at the equalizer input is also required in the DFE analysis. It is proportional to the auto-correlation of the receiver filter,

$$\phi_2(\tau) = \int_{-\infty}^{\infty} f_2(t) f_2(t+\tau) dt . \quad (5)$$

A 4PSK DFE in a non-diversity application is illustrated in Figure 4. In complex notation the impulse responses of the forward and backward filters can be written as

$$w(t) = w_1(t) + jw_2(t), w_1, w_2 \text{ real} \quad (6a)$$

$$b(t) = b_1(t) + jb_2(t), b_1, b_2 \text{ real} \quad (6b)$$

Two comparators compare the analog voltages at the symbol sample time to zero and generate ± 1 outputs on each of I and Q channel in Figure 4. These 4PSK decisions are fed back through the backward filter for cancellation of past intersymbol interference. Because of the discrete nature of the detected symbols the backward filter is a tapped delay line filter with complex tap weights, i.e.,

$$b(t) = \sum_{i=1}^B b_i \delta(t-iT), b_i \text{ complex} . \quad (7)$$

The forward filter must combine matched filtering with ISI removal which suggests the use of a tapped delay line filter with complex tap weights but with less than one 4PSK symbol duration separation, i.e.,

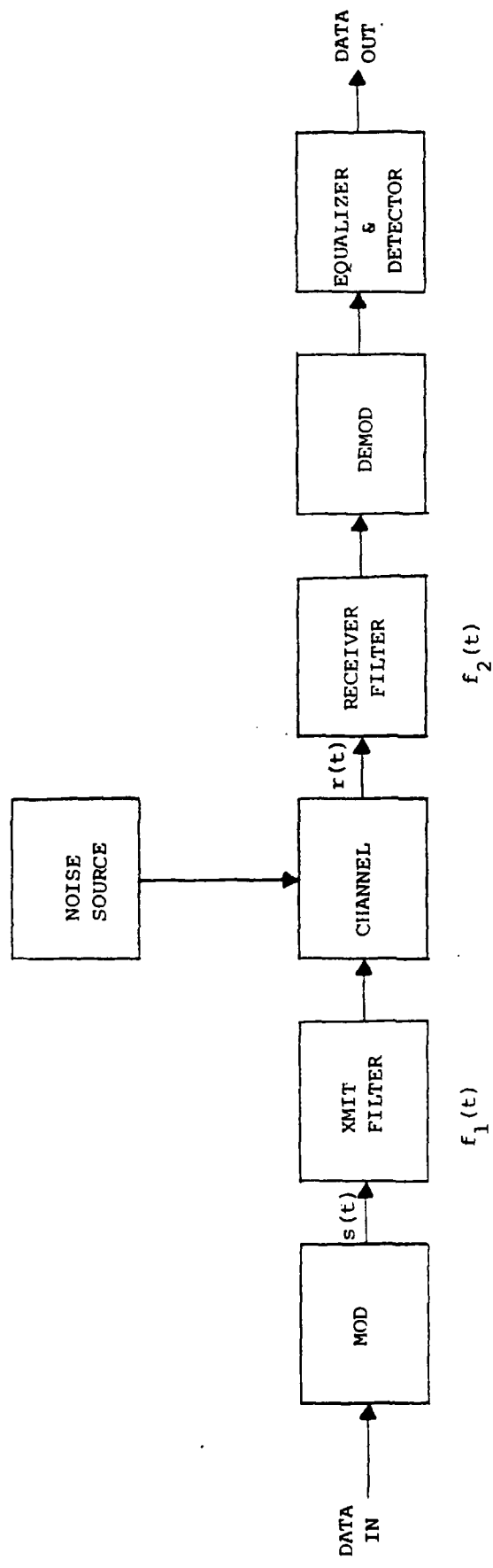


Figure 3 Serial Data Trasmission, Radio System

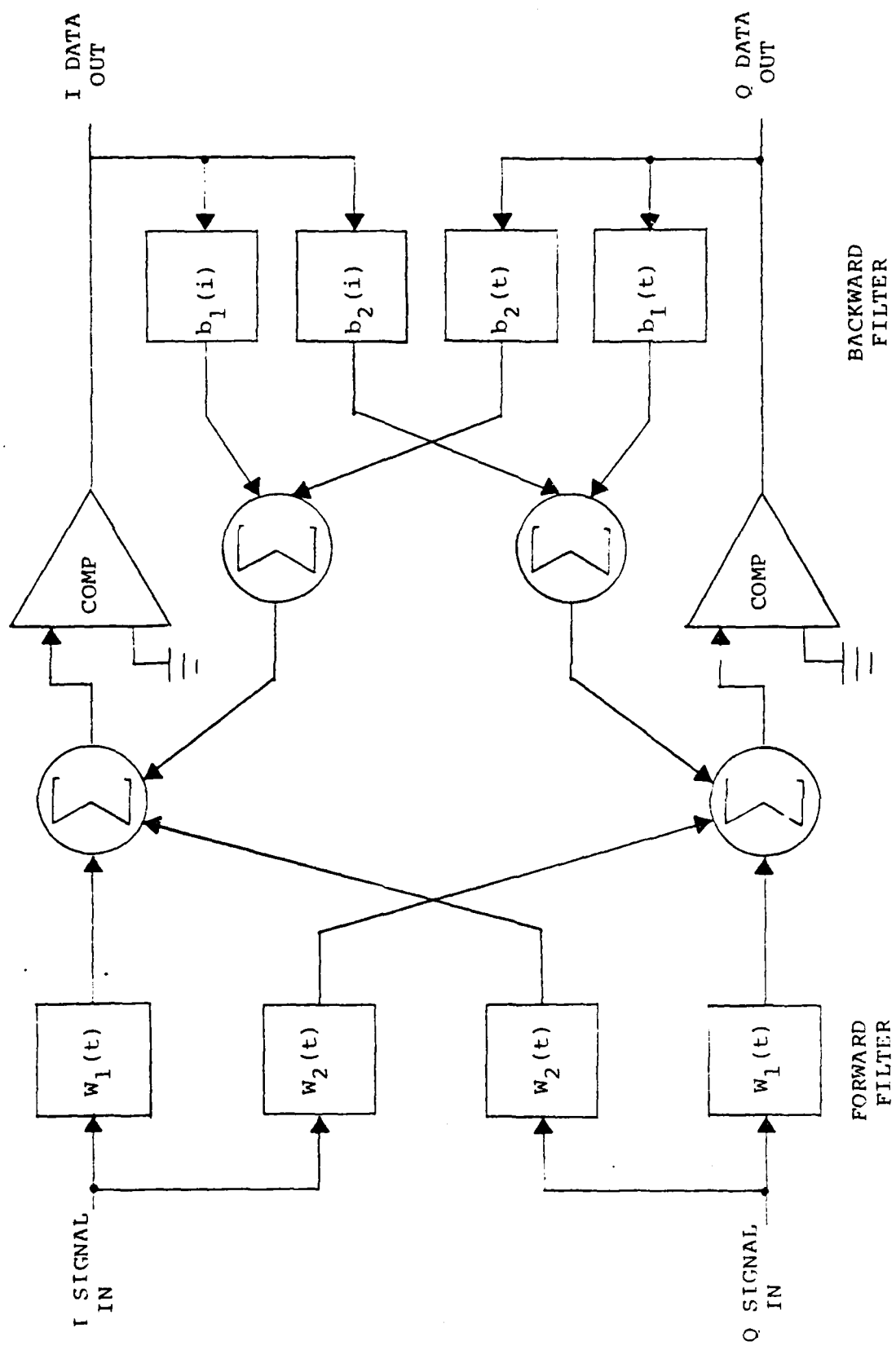


Figure 4 Decision-Feedback Equalizer, 4PSK

$$w(t) = \sum_{k=1}^K w_k \delta(t-t_k), w_k \text{ complex} . \quad (8)$$

The analysis of the DFE under ideal tracking of the fading channel proceeds as follows. Enough backward filter taps are assumed to cancel the past intersymbol interference. The DFE performance then only depends on the number and location (t_k values) of the forward filter. Under perfect tracking conditions, the equalizer performance is summarized in a matrix signal-to-noise ratio S which is of rank K equal to the number of forward filter weights. The equalizer SNR which includes the fading effect is given by

$$S = A^{-1}C \quad (9)$$

where A is the equalizer noise matrix and C is the equalizer signal matrix. For a sampling time t_0 , the signal matrix is given by

$$C_{ij}(t_0) = \int_{-\infty}^{\infty} f(t-t_i) f(t-t_j) Q(t+t_0) dt, i, j = 1, 2, \dots, K \quad (10)$$

The noise matrix includes both an additive noise component and ISI component. The latter is an approximation to a Gaussian noise effect and requires a scale factor ξ which improves the approximation. We have for the noise matrix

$$A_{ij} = N_0 \phi_2(t_i - t_j) + \xi \sum_{j=1}^J C_{ij}(t_0 - jT) \quad (11)$$

where J future ISI interferers have been considered. When the ISI term in (11) is omitted, the SNR matrix defines the no intersymbol interference bound on the DFE performance. The difference between realized performance and this bound is the intersymbol interference penalty.

The eigenvalues of the SNR matrix S are independent implicit diversity signal strengths which satisfy

$$\sum_{k=1}^K \lambda_k < \bar{E}_b / N_0 \quad (12)$$

This transformation which leads to the matrix SNR S also results in uncorrelated noise components with unit power on each implicit diversity channel.

The extension to diversity systems requires consideration of multipath profiles for each diversity, cross multipath profiles representing correlation between diversities, and a parallel forward filter in the DFE for processing of each diversity. If there are D separate diversity types, the matrices S , A , and C are extended to rank DK in an obvious generalization of Equations (9), (10), and (11). The result with diversity is then an equivalent uncorrelated diversity system of order DK with unit power white noise inputs. Since the equalizer SNR matrix corresponds to optimum combining, the equivalent system has the simple form shown in Figure 5.

Compare the detector input in Figure 5 with an ideal QPSK transmission through a white noise channel. In the ideal QPSK system if the received energy per bit is E_b and the noise spectral density is N_0 Watts/Hz, the detector input after matched filtering is

$$\tilde{s}_k = E_b s_k + \sqrt{E_b N_0} n_k . \quad (13)$$

where n_k is a ZMCG noise with unity covariance. The error rate for this ideal system is

$$p = \frac{1}{2} \operatorname{erfc} \sqrt{E_b / N_0} . \quad (14)$$

For the system of Figure 5 we have

$$E_b = \mathbf{g}' \mathbf{g} \quad (15)$$

$$N_0 = 1 . \quad (16)$$

The signal-to-noise ratio

$$\frac{E_b}{N_0} = \mathbf{g}' \mathbf{g} . \quad (17)$$

which determines the instantaneous bit error rate p is the inner product of a Gaussian random vector. The bit error rate is then also a random variable. Depending on the detection system used we have

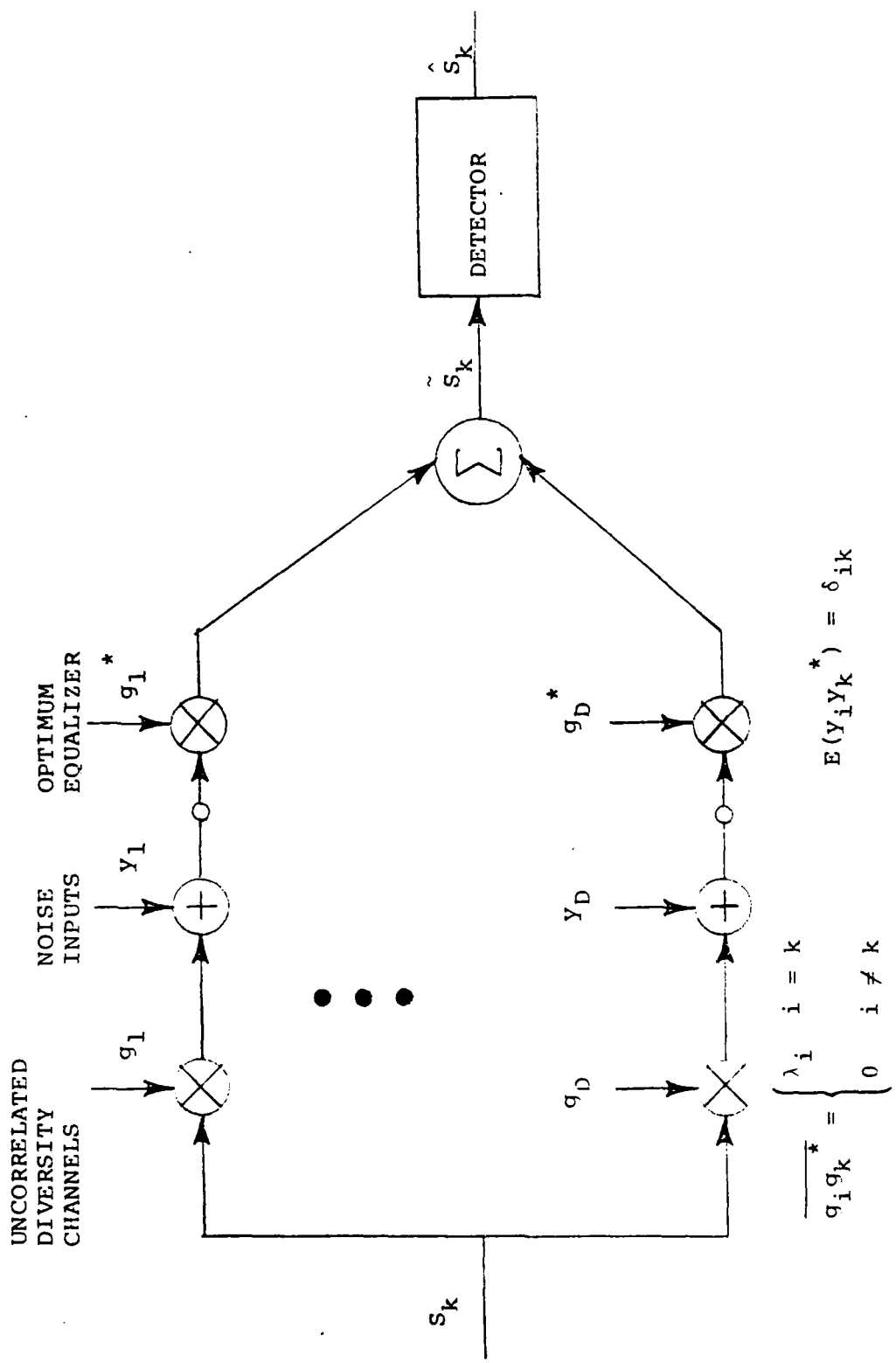


Figure 5 Uncorrelated Diversity Equivalent System

$$p = \frac{1}{2} \operatorname{erfc} \sqrt{\gamma} \quad \text{Coherent Detection} \quad (18)$$

$$p = \frac{1}{2} e^{-\gamma} \quad \text{Differential Detection} \quad (19)$$

In order to obtain the statistics for the bit error rate, it is necessary to obtain the probability density function for the SNR γ .

Because of the components of g are uncorrelated, the transform of the pdf of γ is simply the product

$$p_\gamma(s) = \int_0^\infty p_\gamma(x) e^{-sx} dx = \prod_{i=1}^{DK} \frac{1}{1+s\lambda_i} \quad . \quad (20)$$

By taking the inverse transform, the pdf for γ can be determined and all the BER statistics obtained through the transformations implied by either (18) or (19).

2.3 BEAM CORRELATION AND SQUINT LOSS

Angle diversity is normally only employed at the receiver since the production of multiple transmit beams requires either additional power amplifiers or a reduction in power with power splitters. Thus, conventional angle diversity has one transmit beam and two or more angle of arrival receive beams. More than two beams is also unattractive both because of additional receivers required and the increased squint loss with larger squint angles. Since the diversity advantage stems from the lack of correlation between received diversity signals, the correlation fall-off as a function of squint angle in the vertical and horizontal directions is important in the selection of either vertical or horizontal splayed beams. The power loss fall-off as a function of squint angle is of the same order for the two directions and therefore is not significant in the selection process. The correlation fall-off as a function of squint angle can be related to the correlation distance in the plane of the receive antenna. Spatial correlation parameters at the antenna are related by a Fourier transform to the scattering power density in the common volume defined by the intersection of the two antenna beams. Since Fourier variables in one domain are inversely related to Fourier variables in the other domain, e.g., a short time pulse corresponds to a wide frequency band,

the correlation distance in a particular direction at the receiver is inversely related to the common volume size in that same direction. In Figure 6 we examine the common volume dimensions in the vertical (side view) and horizontal (top view) directions. For angle diversity systems, the transmit beamwidth Ω is typically smaller than the minimum scattering angle θ_0 in order to minimize the loss associated with the squinted beam. The common volume "size" in the horizontal direction is then limited by the transmit beamwidth and is on the order of $\gamma_H r = \Omega r$. In the vertical direction, the common volume "size" is not limited by the transmitter beamwidth as much as the refractive index spectrum fall-off which has a dependence of $\theta^{-11/3}$ where θ is the scattering angle. Since $\theta > \theta_0 > \Omega$ the vertical common volume size $\gamma_V r$ is larger than the horizontal common volume size $\gamma_H r$. The area of useful scattering energy returned to the receiver is figuratively shown in Figure 6 as a shaded area. Since $\gamma_V > \gamma_H$ it follows that the vertical correlation distance will be less than the horizontal correlation distance for narrow beamwidth antennas. Thus the vertical angle diversity system will result in a lower correlation between squinted beams than a horizontal angle diversity system. Experiment results [1,5,6] confirm this theoretical result.

It turns out that as the transmit beamwidth is increased such that $\Omega \gg \theta_0$, the situation reverses and γ_V becomes smaller than γ_H with the result of a smaller horizontal correlation distance than vertical. This result is consistent with "fat" transmitter beam measurements and analysis [20] of correlation distances in the vertical and horizontal planes. However, in any practical application, the transmit beams must be narrow in order to provide the required antenna gain for successful operation.

Because the vertical correlation distance is smaller than the horizontal correlation distance for practical systems, the angle diversity design should utilize a vertical squinted beam as the first additional angle of arrival signal. The use of more angle of arrival signals than two is not advantageous because of system complexity and the diminishing return from additional diversity. Thus in this investigation the system design considered a dual antenna diversity (AD) system with vertically squinted beams.

The angle between the centerlines of the antenna patterns of the two feedhorns in a dual AD system is defined as the squint angle. When the squint angle is appreciably more than a beamwidth, the correlation between the re-

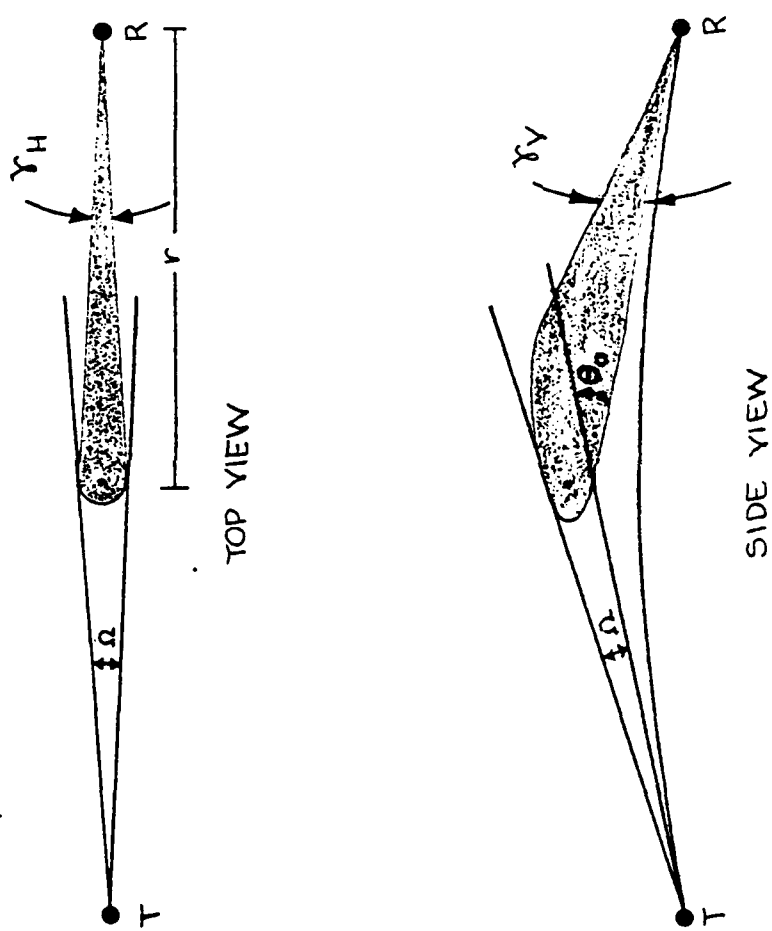


Fig. 6 Troposcatter Path Structure

ceived angle diversity signals is small but the relative signal loss of the elevated beam may be excessive due to the increased scattering angle. Decreasing the squint angle reduces this loss but increases the correlation between diversity signals. The effect of this correlation is to reduce the diversity gain. It becomes necessary to distinguish between narrowband and wideband correlation effects on diversity combining loss. When the diversity signals are smeared by a multipath spread that has width on the order of the reciprocal of the signal bandwidth, the correlation between diversity signals also becomes smeared. Our analysis showed that the diversity combining loss due to diversity beam correlation is less for wideband (\sim on the order of a reciprocal multipath spread) than for narrowband (much less than a reciprocal multipath spread) transmissions.

The digital modem model previously described was used to compute the short term (\sim 1 hour) outage probability as a function of the ratio of mean bit energy \bar{E}_b to noise spectral density N_0 . Outage probability is the probability that the bit error rate (BER) for a particular "frozen" segment of the fading ensemble is greater than 10^{-4} . The outage probability then represents the fraction of intervals on the order of 1 second where the BER is greater than 10^{-4} . The results of the outage probability calculations for example* C-band (4.4 - 5.0 GHz) and L-band (255-985 MHz) links are shown in Figures 7 and 8. These curves reflect the effects of both squint loss and diversity correlation as a function of squint angle measured in beamwidths (BW). The two examples have approximately the same main beam multipath spread. ($2\sigma_{MB}/T = 0.45$). Figure 7 represents the RADC Youngstown-Verona test link while Figure 8 is the DCS Sahin Tepesi-Yamanlar link.

We can now isolate the wideband correlation loss by noting that the diversity loss in the absence of correlation is approximately one-half the squint loss. Performance measures with unequal branch SNR in dB are well approximated by the geometric mean of the SNR or the arithmetic mean in dB. Thus by comparing the diversity loss of specific squint angle cases with a case with zero correlation coefficient, the wideband correlation loss can be computed from the curves of Figures 7 and 8. Plots of the correlation coef-

* Non detailed parameter specifications for these links are given in Section 4.1, Table 2.

Fig. 7

Outage Rate for C-band Link

MODEL

DATE

OUTAGE RATE: PROBABILITY BER EXCEEDS 10^{-4}

46 6463

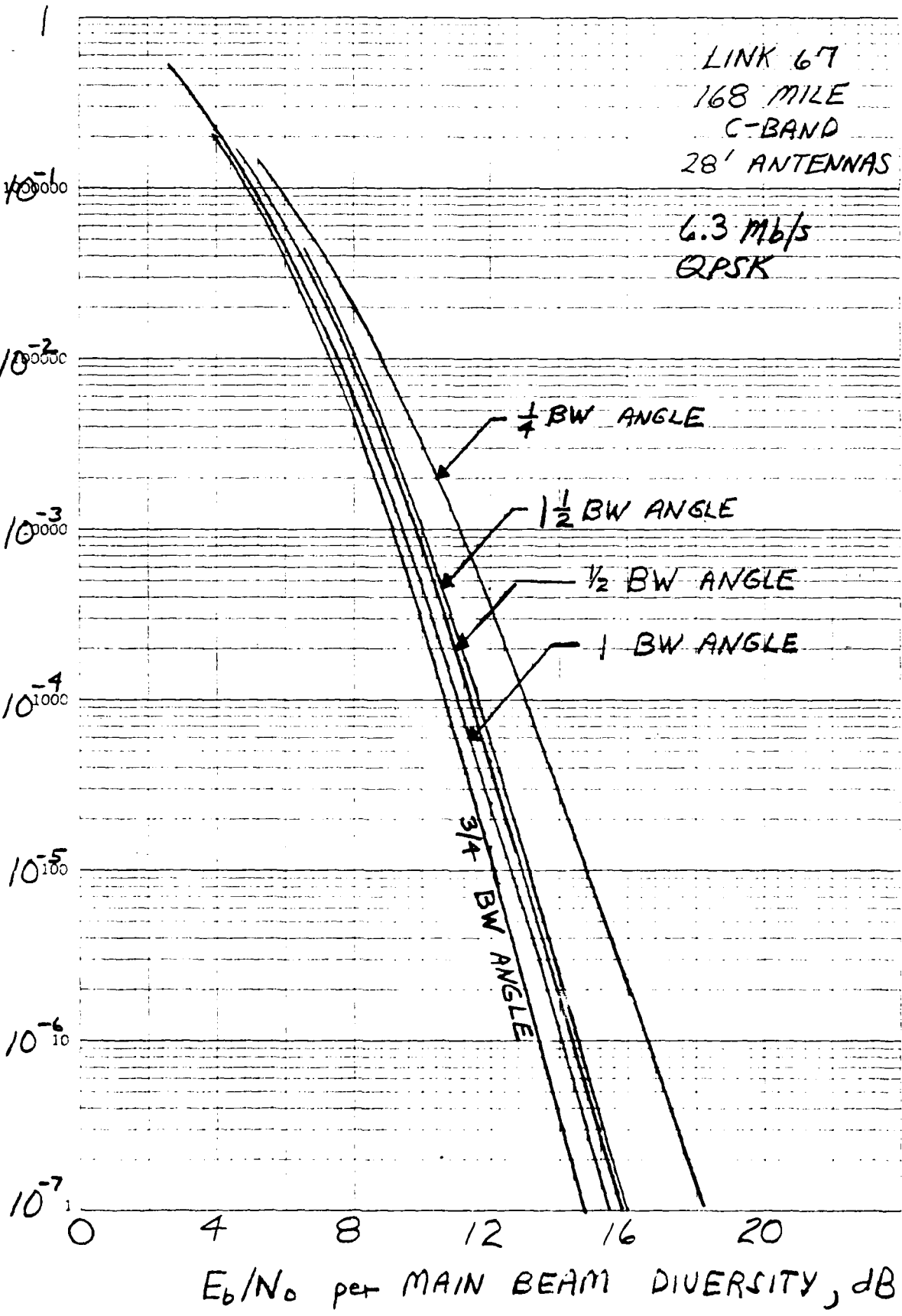
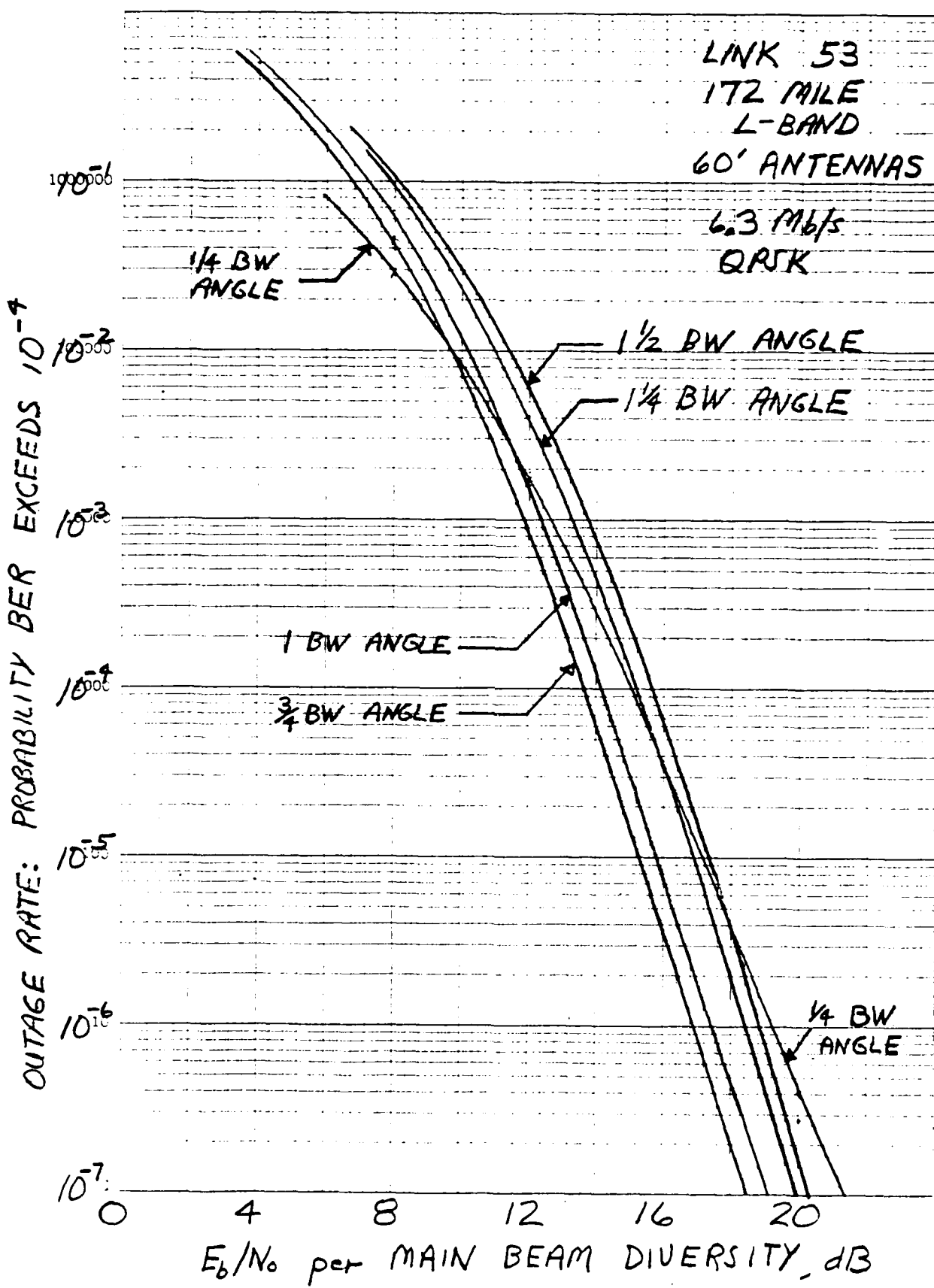


Fig. 8 Outage Rate for L-band Link

MODEL

DATE



46 6463

KEY: SAME AS IN FIGURE 7, EXCEPT FOR 60' ANTENNAS

ficients and the wideband and narrowband correlation losses are given in Figure 9 for the C-band example. The L-band result is similar. The reduced effect of correlation between angle diversity branches with wideband signaling is due to an adaptive equalizer modem [11,12] which acts to combine individual multipath components on diversity pairs. These individual multipath components have less correlation than the correlation from the cumulative multipath structure.

In these examples and all others computed, the optimum squint angle was determined to be approximately 1 beamwidth for narrowband signaling and 3/4 beamwidth for wideband signaling. Thus, it is clear that the best squint angle for megabit data rates in angle diversity systems is less than one beamwidth. Feedhorn design constraints, however, make it difficult to achieve squint angles this small. Fortunately, the dB loss is small for squint angles larger than 3/4 beamwidth. Because of the feedhorn design problem, this result has important practical implications. The feedhorn design for the RADC test link used in this investigation resulted in the measured squint angles given in Table 1. Vertical polarization is used for signal reception in the RADC tests. The additional loss for this link resulting from a squint angle larger than 3/4 beamwidth can be determined from Figure 7 to vary between 0.3 and 0.8 dB.

Table 1
Test Link Squint Angles

	Right Antenna		Left Antenna	
	H Pol.	V Pol.	H. Pol.	V. Pol.
Squint Angle	0.65°	0.73°	0.55°	0.68°
Half-Power Beamwidth	0.55°	0.53°	0.50°	0.50°

2.4 ANTENNA POINTING ANGLE

The question of boresight/horizon angle, i.e., the angle between the main beam antenna pattern centerline (boresight) and the horizon is complicated by the presence of two received beams in an angle diversity configuration. As this pointing angle is decreased, the relative loss of the elevated

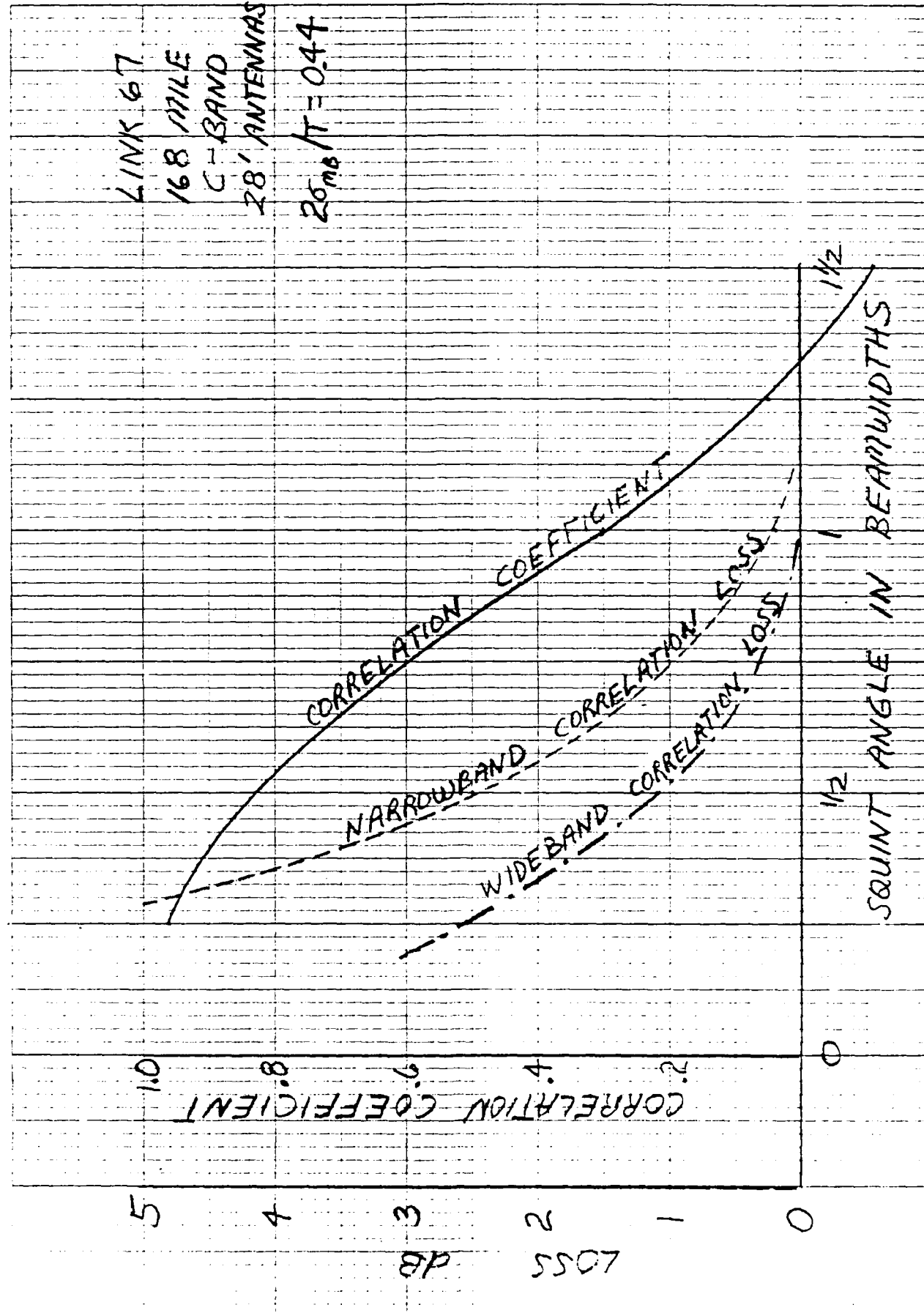


Fig. 9 Correlation Loss, C-band link

beams is reduced but more of the main beam pattern is blocked by the radio horizon. Thus an optimum angle exists. Since operational angle diversity system are utilized in both directions, the boresight/horizon angles at transmitter and receiver are constrained to be equal in the optimization search. Using a squint angle of one beamwidth*, the main beam loss for a conventional system was determined as a function of antenna pointing angle and in addition the diversity combining loss due to squint loss and narrowbeam correlation was computed. The minimum of the sum of these losses was used as the criterion for determining the optimum pointing angles. The results showed that the optimum boresight/horizon angle for the transmit and receiver antennas was found to fall between 1/4 and 1/2 beamwidth elevation above the local horizon. This result was only slightly influenced by the frequency of operation since lower frequency systems usually use larger antennas.

The major effect in the optimization is the rapid increase in main beam loss when earth blockage begins to occur. For this reason correlation and squint loss have a small effect on the choice of optimum pointing angle. This large dependence on main beam blockage also establishes that the optimum pointing angles for conventional and angle diversity systems are approximately the same. Although other researchers have suggested in the past that an attempt to equalize the main and elevated beams is desirable, these results show that the main beam blockage from such a strategy would lead to an overall degradation. Under homogeneous atmospheric conditions, when the main beam signal is maximized, the elevated beam signal will be somewhat smaller. The frequent occurrence of nonhomogeneous atmospheric conditions causes the elevated beam signal to be stronger than the main beam signal. This phenomenon makes it necessary to aim the antenna system with a series of tests extending over a least several days in order to preclude pointing the antenna into the ground as a result of nonhomogeneous atmospheric conditions. For this reason, it is likely that many DCS troposcatter antenna systems are aimed too low and 2 or 3dB could be gained by careful aiming techniques.

A final consideration in choice of antenna/horizon angle is the effect of increased multipath in both beams due to larger pointing angles. Because digital modems can utilize the multipath to increase the effective diversity

* The design goal for the feedhorn.

order if the multipath spread is not too large, it is advantageous to choose a somewhat larger pointing angle if the nominal multipath spread is small compared to the data symbol interval. However, for L-band systems the multipath spread, particularly in the elevated beam, may exceed the multipath capabilities of the digital modem. In this situation degraded performance due to intersymbol interference results.

In summary an optimized angle diversity system utilizes a squint angle of approximately $3/4$ beamwidth with a boresight/horizon angle approximately equal to $1/2$ beamwidth for C-band digital systems and somewhat less than $1/4$ beamwidth for L-band systems. Under homogeneous atmospheric conditions this configuration results in less received signal power in the elevated beam. The use of pointing angles at much less than $1/4$ beamwidth is suboptimum because too much power is blocked in the main beam by the radio horizon.

SECTION 3
TROPOSCATTER PATH PREDICTION TECHNIQUE

The prediction of the performance of angle diversity or any diversity system requires the formulation of a transmission loss model. This model is used to compute the median path loss and multipath statistics. A variability model is then required to predict the effect of yearly variations in these parameters. In our investigation a new approach to the calculation of transmission loss and multipath statistics was developed. This approach includes the effects of aperture to medium coupling loss. In addition, the effects of long term variations of received signal level are considered for angle diversity systems.

3.1 BACKGROUND

Theory and practical techniques for troposcatter communication started developing around 1950 [14]. Two main theories have been proposed, the layer reflection theory [15] and the turbulent scattering theory based on the turbulence results developed by Obukhov and Kolmogorov in 1941 [16]. Initially, various layer reflection theories received the most attention, partly because the predicted behavior was close to the observed linear dependence of the scattering cross-section with wavelength. The layer reflection theory also predicts a dependence on the scattering angle close to the empirically determined dependence of the form θ^{-5} . In later years, experiments at higher frequencies and with narrower antenna beams [17,18] have indicated the applicability of the turbulence theory, with a scattering angle dependence of the form $\theta^{-11/3}$ and a wavelength dependence for the scattering cross-section of the form $\lambda^{-1/3}$. In practice layer reflection and scattering will exist simultaneously with layer reflection being more frequent when widebeam antennas and low frequencies are used. Experimental results [17] indicate that the wavelength dependence can vary between λ^{-1} and λ^3 . The scattering angle dependence has been measured to lie in the range c: θ^{-2} to θ^{-6} [19]. The exponent in the scattering angle is frequently called the refractive index spectrum slope since it also indicates the fall-off of the wave number spectrum of the refractive index, provided the wavelength is in the so-called inertial subrange, i.e., between the inner and outer scale of turbulence.

A number of theoretical and computational models have been developed [14,16,21,22,23]. Further references and a discussion of these models can be found in Larsen, [24] or Panter, [25]. The most generally accepted model is that of NBS [21,22] which, based on a large number of empirical results, assumes the refractive index spectrum slope is five. Several arguments can be forwarded in support of using a spectrum slope of 11/3 instead. First, the trend is toward troposcatter links at higher frequencies where layer-reflection is less important. Second, on links with both turbulent scatter and layer reflection the turbulent scatter is the more critical effect since during the worst days, communication will be by scatter only and layer reflection, when present, tends to increase the received power.

3.2 PROPAGATION MODEL SUMMARY

Radiowave propagation in the troposphere is determined by the refractive index. The refractive index can be described by its short-term mean and variance, both of which are highly dependent on geographic location, season, and time of day. The mean refractive index is usually linearly decreasing as a function of height, and can be handled by defining an effective earth radius.

The refractive index fluctuations are characterized by the covariance function. If $n(\underline{r})$ is the refractive index at a point with coordinates \underline{r} then define

$$n_1(\underline{r}) = n(\underline{r}) - E[n(\underline{r})] , \quad (21)$$

and its covariance function

$$\phi_n(\underline{r}_1, \underline{r}_2) = E[n_1(\underline{r}_1) n_1(\underline{r}_2)] . \quad (22)$$

In a homogeneous medium this covariance is only a function of $\underline{r}_1 - \underline{r}_2$, and in such a case the wavenumber spectrum is defined by

$$\Phi_n(\underline{k}) = \frac{1}{(2\pi)^2} \iiint \phi_n(\underline{r}) e^{-i\underline{k} \cdot \underline{r}} d^3 \underline{r} . \quad (23)$$

For the isotropic atmosphere the wavenumber spectrum is only a function of the magnitude k of the wavenumber vector \underline{k} . The wavenumber spectrum is important

since it has been shown [Tatarskii, 1971] that the scattering cross-section (a_s) of a small volume (dV) is

$$a_s = 8\pi^2 k^4 \phi_n \left(2k \sin \frac{\theta}{2}\right) dV, \quad (24)$$

where θ is the scattering angle. The wavenumber spectrum is usually modeled by the von Karman spectrum [16]

$$\phi_n(k) = \frac{\Gamma\left(\frac{m}{2}\right)}{\pi^{3/2} \Gamma\left(\frac{m-3}{2}\right)} \sigma_n^2 r_0^3 (1 + k^2 r_0^2)^{-m/2}, \quad m > 3 \quad (25)$$

If $\phi_n(k)$ is plotted on a doubly logarithmic scale against the wavenumber k , the slope falls off as m , so that m is called the spectrum slope. σ_n^2 is the variance of the refractive index and r_0 is the correlation distance of the turbulence. The power received from a small scatterer at a point \underline{r} and with the cross-section a_s is

$$dP_R(\underline{r}) = P_T \cdot \frac{G_T(\underline{r})}{4\pi R_T^2(\underline{r})} \cdot \frac{a_s(\underline{r})}{4\pi R_R^2(\underline{r})} \cdot \frac{\lambda^2 G_R(\underline{r})}{4\pi} \quad (26)$$

where

$P_T(P_R)$ = Transmitted power (received power)

$G_T(\underline{r}) (G_R(\underline{r}))$ = Gain of transmitter (receiver) antenna toward the scattering point \underline{r} .

$R_T(\underline{r}) (R_R(\underline{r}))$ = Distance from transmitter (receiver) to the scattering point \underline{r} .

Using the expression for the scattering cross-section and the von Karman spectrum assuming

$$kr_0 \gg 1 \quad (27)$$

it is found that the received power is

$$P_R = P_T \cdot C \iiint_V \frac{G_T(\underline{r}) G_R(\underline{r})}{R_T^2(\underline{r}) R_R^2(\underline{r})} \left(2 \sin \frac{\theta(\underline{r})}{2} \right)^{-m} d^3 \underline{r} \quad (28)$$

where

$$C = \sigma_n^2 r_0^{3-m} \Gamma \left(\frac{m}{2} \right) / \left(2\sqrt{\pi} \Gamma \left(\frac{m-3}{2} \right) \right), \quad (29)$$

and the range of integration, V , is the total common volume. It is assumed that σ_n^2 and r_0 do not vary appreciably throughout the common volume.

While the Kolmogorov-Obukhov theory of turbulence predicts $m=11/3$, the above expression can be used formally for other values of m . In particular, setting $m=5$ yields the expression used by the NBS model [21]. In order to predict the received power P_R it is necessary to specify m , r_0 and σ_n^2 . We take r_0 equal to L_0 , the outer scale of turbulence. The value of L_0 found by Fried [26] was

$$L_0 \sim 2\sqrt{h} \cdot 1 \text{ meter} \quad (30)$$

where h is the height of the air mass. It must be emphasized that considerable variation from this value of L_0 can be expected under different atmospheric conditions. Measurements and predictions of σ_n^2 have been presented by numerous authors [18,26,27]. At radio frequencies, the variance σ_n^2 is strongly dependent on the humidity. For the dry atmosphere, measurements at radio- and at optical-frequencies yield nearly identical values of σ_n^2 . Since dry atmosphere represents the worst case for radio wave scatter measurements, it will often be possible to apply optical results to the study of tropo-scatter at radio frequencies. This is useful since many more measurements have been made of the optical refractive index than of the radio refractive index. Fried [26] suggested the following model of the optical refractive index variance:

$$\sigma_{n,\text{opt}}^2 = 6.7 \cdot 10^{-14} e^{-h/3200} \text{ m} \quad (31)$$

New results indicate a stronger height dependence [27,28], particularly for continental air masses.

σ_n^2 is the main source of variability in received signal levels, so a complete description of σ_n^2 variation versus weather, time-of-day, season, location, etc., is therefore desirable. Unfortunately, only sporadic measurements have been made. Gossard, [27] has calculated both optical and radio refractive index variations of several classes of air masses. Using this method, profiles of σ_n^2 (or the structure constant C_n^2) can be calculated as a function of geographic location, season, and time-of-day. Radiosonde data can also be used to predict the variance σ_n^2 for a troposcatter link using a formula by Tatarskii, [16], and Sirkis [29]. Typical values of σ_n^2 at heights of 2km or below are in the range 10^{-14} to 10^{-13} . The propagation model in this effort used Fried's model given by Equation (31) for computing the median path loss.

The median path loss is obtained in this model by integrating the differential received power (26) over the common volume defined by the intersection of the transmit and receive antenna patterns. In a dual vertical angle diversity system, there are two such common volumes one for the intersection of the main beam and one for the intersection of the transmit beam and an elevated receive beam. The multipath profile is obtained by performing the integration over individual regions of constant path delay. For the wide sense stationary, uncorrelated scattering channel the result of these integrations can be expressed in terms of the statistic of the random impulse responses of the diversity channel, i.e.,

$$\text{Main Beam: } h_m(t) h_m^*(\tau) = Q_m(t) \delta(t-\tau) \quad (32)$$

$$\text{Elevated Beam: } h_e(t) h_e^*(\tau) = Q_e(t) \delta(t-\tau) \quad (33)$$

The multipath profile or delay power spectrum is $Q_m(t)$ or $Q_e(t)$ for the main or elevated beam, respectively. The common volume integrations for a constant path delay give $Q(t)$ directly. The median received powers and 2 σ multipaths spread are given by

$$P_m = \int_0^{\infty} Q_m(t) dt \quad (34)$$

$$P_e = \int_0^{\infty} Q_e(t) dt \quad (35)$$

$$\sigma_m^2 = \frac{1}{P_m} \int_0^{\infty} t^2 Q_m(t) dt - \left[\frac{1}{P_m} \int_0^{\infty} t Q_m(t) dt \right]^2 \quad (36)$$

$$\sigma_e^2 = \frac{1}{P_e} \int_0^{\infty} t^2 Q_e(t) dt - \left[\frac{1}{P_e} \int_0^{\infty} t Q_e(t) dt \right]^2. \quad (37)$$

A cross multipath profile $Q_{me}(t)$ is also calculated by numerical integration in order to assess the correlation between the main and elevated diversity signals. The correlation profiles are obtained similarly, except that instead of a single receiver antenna power gain factor $G_R = |g_R(\underline{r})|^2$, two separate voltage gain factors $g_{R_1}(\underline{r})$ and $g_{R_2}^*(\underline{r})$ are used. These are defined as complex gains whose phase angle is the actual RF phase shift from the scatterer at \underline{r} to the antenna location. The effectively random RF phase relationship between the signal paths from a given scattering point \underline{r} to two distinct receiver antenna locations is the primary cause of decorrelation of the resultant signals at the two antennas.

Aperture-to-medium coupling loss [25] which is a loss associated with the illumination of only a fraction of the total scattering volume is included in the path loss calculation by integration over the antenna pattern amplitude distribution. Semi-empirical or approximation techniques are not required to derive this loss factor.

For convenience closed form results for the path loss and aperture-to-medium coupling loss have been derived [30]. These results provide good agreement (generally within 1 or 2dB) with the more exact numerical integration method.

3.3 LONG TERM VARIABILITY

Tropospheric scatter systems are subject to two fading phenomena - short term multipath fading and long term power fading. The short term fading of the instantaneous received power within periods of time ranging from less than a second to many minutes results from random fluctuations in the relative

phasing between component waves arriving at the receiver over slightly different propagation paths. The long term power fading results from slow changes in average atmospheric refraction, in the intensity of refractive index turbulence, and in the degree of atmospheric stratification. The power fading is characterized by hourly or diurnal variations. The evaluation of troposcatter system performance is accomplished in part by determining the hourly median path loss where the median is computed to include the short term multipath fading and in turn considering the median path loss as a random variable subject to a power fading distribution. The median path loss calculation utilizes fixed values of the mean and variance of the refractive index and an assumption on the degree of atmospheric stratification. In the previous section we have summarized a prediction method for the computation of median path loss and multipath spread. This method has the following important characteristics:

- The average atmospheric refraction is fixed by utilizing an effective earth's radius of K times the actual radius to account for the mean refractive index.
- The intensity of refractive index turbulence is fixed by the refractive index variance which is chosen to correspond to dry winter afternoons. This period of time generally experiences the poorest propagation conditions.
- The atmospheric structure is derived from turbulent scattering theory which leads to a refractive index spectrum slope of $m=11/3$. This structure is more applicable for higher frequency ($> 1\text{GHz}$) troposcatter systems than the stratified layer assumption used in the NBS prediction method ($m=5$).
- The aperture-to-medium coupling loss is included as an integral part of the path loss calculations.

For this method the power fading of the median path loss is determined by variations in the effective earth radius factor K , variations in the refractive index variance σ_n^2 , and changes in the atmospheric structure leading to other values of the refractive index spectrum slope m . Given probability density functions on the parameters K , σ_n^2 , and m , the computation of the median path loss long term distribution would be straightforward. Unfortunately there is little empirical data available to derive such densities. Some experimental evidence and analysis [27] indicate that the refractive index

variance σ_n^2 is the dominating factor in producing significant variations in the median path loss. Development of experimental data on σ_n^2 over long periods of time for different geographical areas would provide a basis for predicting long term variability of troposcatter systems. At the present time the only method of predicting this variability is to use path loss data taken from existing systems and integrated into the NBS variability model [21]. Much of the empirical path loss data has been taken from systems with operating carrier frequencies below 1GHz. The performance prediction for new troposcatter systems operating in the 4 to 5GHz frequency region may be subject to large errors as a result. However, in the absence of empirical data on either σ_n^2 or median path loss at these new frequencies, an extrapolation of the NBS variability model is the only realistic engineering choice. We first briefly review the NBS model and then evaluate the long term variability of an angle diversity system.

3.3.1 NBS Long Term Variability Model

Considerable experimental evidence suggests that the long term distribution of the hourly median path loss is normally distributed in dB. If we denote $L(p)$ as the hourly median path loss in dB, which is not exceeded p% of the time, the normal distribution is defined as follows: -

$$\frac{p}{100} = \text{prob}\{\text{median path loss} < L(p)\}$$

$$= \frac{1}{\sigma_L \sqrt{2\pi}} \int_{-\infty}^{L(p)} \exp\left[-\frac{(\xi - L(50))^2}{2\sigma_L^2}\right] d\xi. \quad (38)$$

where $L(50)$ is the median path loss computed using the numerical integration of (26) and σ_L is the long term standard deviation. The NBS Long Term Variability Model [Rice, 1967] uses empirical data to determine $L(10)$ and $L(90)$ from which normal probability graph paper can be used to plot $L(p)$ at other values of p. This calculation includes the effect of prediction uncertainty through a parameter called service probability. The service probability is the probability that a new system will meet the long term performance predictions.

The path loss distribution corresponds to a service probability of 50%, i.e., 50% of the systems built would exceed the performance predictions.

Present engineering practice recommends the selection of a service probability of 95%. For this choice the loss distribution must be adjusted by the prediction error according to the NBS formula

$$L_{0.95}(p) = L(p) + 1.65 \sqrt{12.73 + 0.12Y^2(p)} . \quad (39)$$

The mean E_b/N_0 distribution for evaluating long term variations in digital system performance is determined from the path loss distribution by the formula

$$\frac{E_b}{N_0}(p) = P_T + G_T + G_R - L_{.95}(p) - [10 \log (R_b) + NF - 174] + 1.6 \quad (40)$$

where

P_T = transmit power in dBm

G_T = transmit antenna gain in dB

G_R = receiver antenna gain in dB

$L_{.95}(p)$ = path loss not exceeding p% of the time for unit gain antennas* and a service probability of 0.95.

$Y(p)$ = long term variability of hourly median path loss

R_b = data rate in b/s

NF = receiver noise figure in dB

-174 dBm = received noise power in 1Hz bandwidth

1.6 dB = factor relating median to mean for a complex Gaussian scatter channel.

* Aperture to medium coupling loss of the actual diameter antennas is included in this parameter.

3.3.2 Long Term Variability in an Angle Diversity System

In space and frequency diversity systems, the common scattering volume is virtually the same for each diversity and hence the long term median path loss varies the same for each diversity. In angle diversity systems, however, the common volumes are separated and the long term variability is not identical for the angle diversity beams. The effect of this decorrelation of the diversity power fading may improve the system availability because a power fade in the main beam diversity is not always accompanied by a power fade in the squinted diversity beam. Physically one can imagine this situation in a vertical angle diversity system where the inhomogeneous structure of the atmosphere results in say a larger refractive index variance or superior atmospheric stratification at heights corresponding to the elevated beam than at heights defined by the main-beam common volume. Since the common volumes in a vertical angle diversity system are separated by approximately one beamwidth Ω at a distance $d/2$ from the link terminals, this decorrelation results from atmospheric variations over distances on the order of $\Omega d/2$. For typical troposcatter applications this distance is on the order of one or more miles at a height above the earth's surface also on the order of a few miles. Experimental evidence verifying the long term power fading decorrelation in angle diversity systems has been reported on by Monsen [31] and Troitskiy [32]. Data from these angle diversity experiments and data from our angle diversity field tests have been used to establish that a significant advantage for angle diversity derives from this effect [13].

The prediction model incorporates this effect in the following way. The outage probability $p_0(x_1, x_2)$ where x_1 and x_2 are the main diversity SNR values in dB for the main and elevated beams is approximated by

$$p_1(\bar{x}) \equiv p_0(\bar{x}, \bar{x}), \quad \bar{x} = (x_1 + x_2)/2 \quad . \quad (41)$$

This approximation is motivated by the fact that outage probability for values much less than unity is well approximated by the arithmetic mean of the diversity SNR values in dB. The yearly average outage probability is then determined by integration over the joint normal density function, f_2 ,

$$\bar{p}_1 = \int_{-\infty}^{\infty} \int_{-\infty}^{\infty} p_1(\bar{x}) f_2(x_1, x_2 | u_1, u_2, \sigma_1, \sigma_2, p) dx_1 dx_2 \quad (42)$$

where $u_i, \sigma_i, i=1,2$, are the main and elevated beam yearly mean RSL and standard deviations. The parameter P is the long term correlation coefficient. After a change of variables to \bar{x} in (42), a one dimensional integral results. One has

$$\bar{p}_1 = \int_{-\infty}^{\infty} p_1(\bar{x}) f_1(\bar{x} | u_e, \sigma_e) d\bar{x} \quad (43)$$

where the effective mean and standard deviation are

$$u_e = (u_1 + u_2)/2 \quad (44a)$$

$$\sigma_e = (\sigma_1^2 + 2P\sigma_1\sigma_2 + \sigma_2^2)/4 \quad (44b)$$

The reduction in the standard deviation σ_e due to the correlation coefficient P is responsible for the long term angle diversity advantage. The model assumes $\sigma_1 = \sigma_2$ (this is a pessimistic assumption as the refractive index variance decreases with height which would tend to reduce σ_e further) and an exponential decrease in P as a function of the height difference between the common volumes.

SECTION 4
PREDICTED AND MEASURED RESULTS

The prediction model which includes modem performance, median path loss, and long term variability has been used to predict link performance of all existing DCS and NATO troposcatter links. These prediction results are given in a separate Link Assessment Report [33]. A laboratory simulation test program and a field test program were used to provide empirical results as a preliminary evaluation of the prediction model and to assess equipment capabilities. The laboratory simulation included tests of a four port Pre-Detection Combiner (PDC) which was used to augment the quadruple diversity MD-918 DFE modem to provide an eighth order diversity capability. The field tests were designed to provide path loss and multipath spread data over an extended period of time and to evaluate digital transmission angle diversity configurations. In particular the field tests compared frequency and angle diversity and they evaluated the augmentation of a conventional 2S/2F system with angle diversity to produce eighth order 2S/2F/2A system. The detailed laboratory and field test results are given in the Test Report [34].

4.1 TROPOSCATTER LINK RESULTS

A major objective of the prediction analysis was to develop long term performance estimates for digital troposcatter systems. The prediction model described in Section 3 contains a propagation analysis, modem component, and long term, i.e., yearly, variability estimate. Performance is compared against the DCS objective of an average outage probability in a call minute at a 10^{-4} BER threshold. The prediction model computes both the outage probability, i.e., the probability that the BER during any short interval (~ 1 second) is worse than 10^{-4} , and also the fade outage per minute which is the probability that the short interval BER will exceed 10^{-4} sometime during a minute interval. These probabilities are then averaged over the yearly path loss variations. The DCS objective for the fade outage per minute is 7.5×10^{-4} for the entire year.

As an example of prediction results, the two troposcatter links used in Section 2 to evaluate angle diversity design features have been analyzed and the long term performance estimates are given in Figures 10 and 11. Path parameters for these links are summarized in the table below.

K-E SEMI-LOGARITHMIC 7 CYCLES X 10 DIVISIONS
KEUFFEL & ESSER CO., MADE IN U.S.A.

46 6460

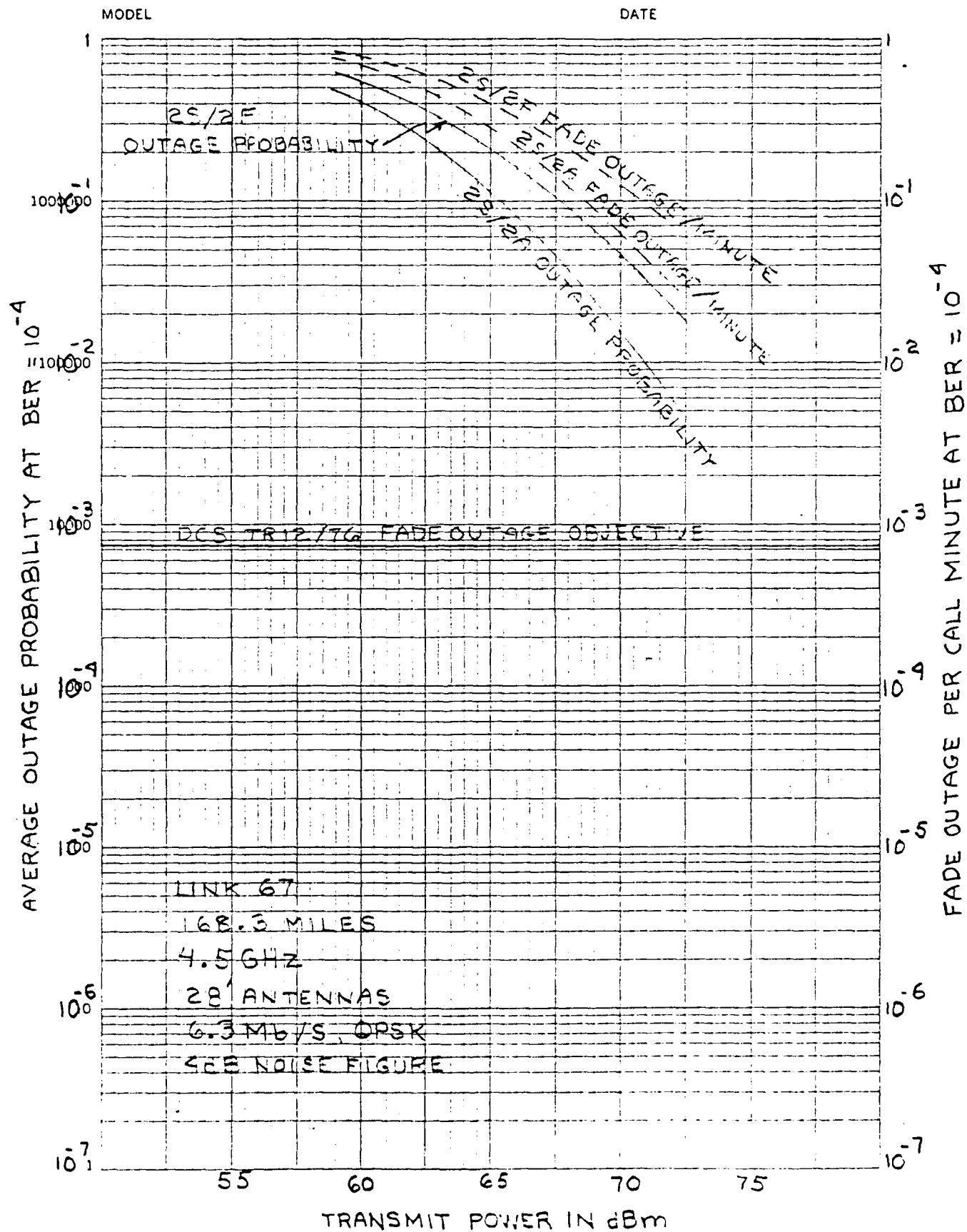


Figure 10 Predicted Outage Probability, RADC Link

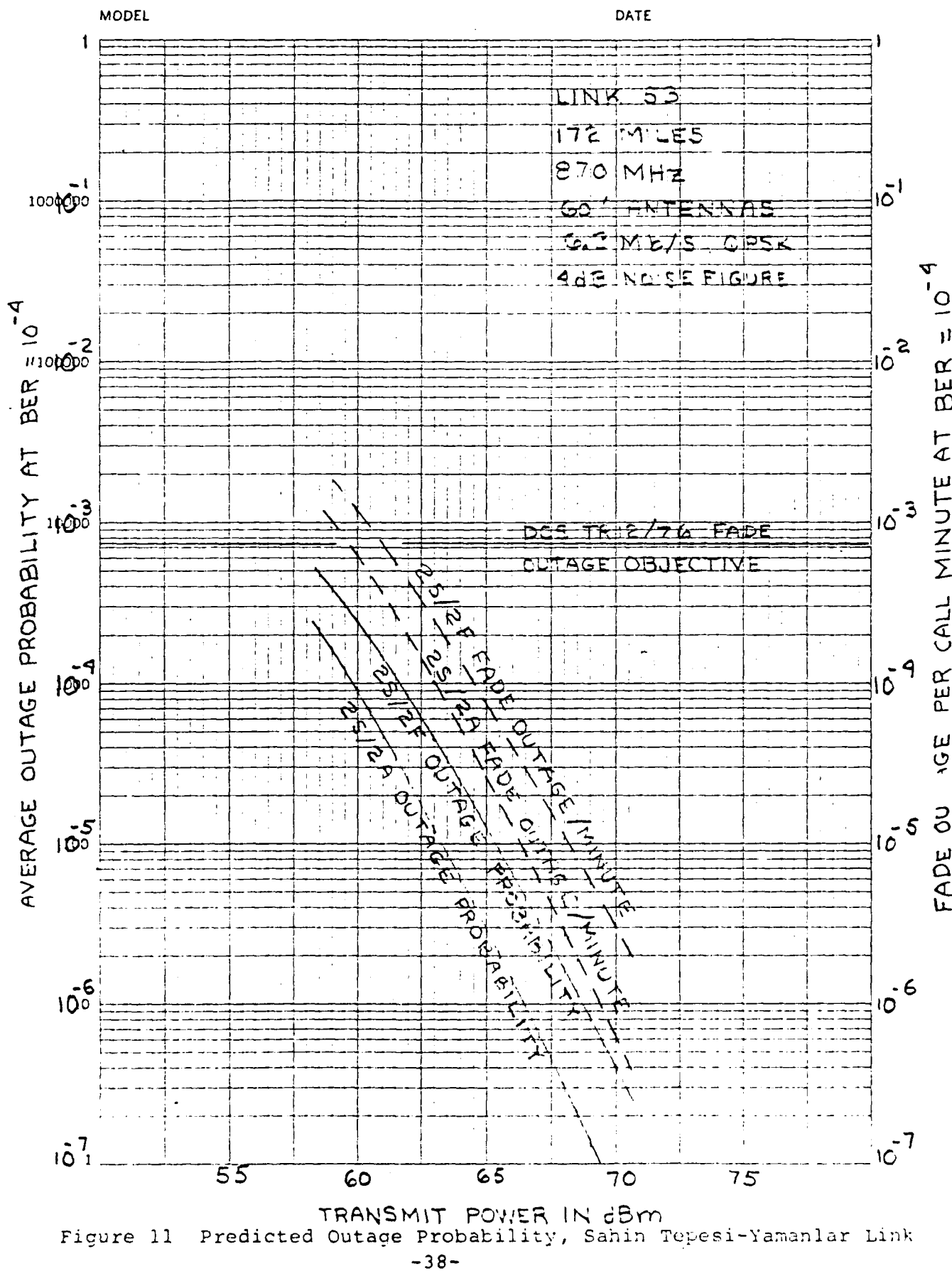


Figure 11 Predicted Outage Probability, Sahin Tepesi-Yamanlar Link

Table 2
Path Parameters

PATH	Link 67 (RADC Link)	Link 53
	YOUNGSTOWN-VERONA N.Y.	SAHIN TEPESSI-YAMANLAR
Length	168 s.m.	172 s.m.
Antennas	28' - 28'	60' - 60'
Frequency, GHz	4.6	0.85
3 dB Beamwidth	0.54° - 0.54°	1.3° - 1.3°
Station Elevation	320' - 440'	2893' - 3176'
Antenna Height	20'/20' - 20'/20'	70'/70' - 82'/82'
Take-off Angle	0.28° - 0.28°	0° - -.21°
Scatter Angle	1.8°	1.7°

The modem used in the analysis is the DFE modem (MD-918) described earlier. The results are presented for Dual Space/Dual Frequency (2S/2F) and Dual Space/Dual Angle (2S/2A) diversity systems. These prediction results include the long term variability improvement for angle-diversity using the method described in Section 3. These improvements are estimated to be 10 dB and 2 dB for the C-Band (Link 67) and the L-Band (Link 53) systems, respectively. The long term correlation coefficients between main beam and elevated beam median signals was measured as 0.7 on the C-band link and estimated from the height geometry on the L-band link.

The C-band system is a test link and not a DCS link. The length of this link and relatively large take-off angles result in inadequate performance relative to the DCS objective. Field test results support this conclusion. Predicted and measured results are summarized in the following table. A nominal 2KW transmitter power is assumed.

Table 3

	Predicted	Measured
Median Main Beam RSL	-96.7 dBm	-94.1 dBm
Median Elev. Beam RSL	-93.3 dBm	-97.4 dBm
Median RSL Std. Dev.*	5.2 dB	6.9 dB

Since the RSL standard deviation has a generally greater impact on link performance than median RSL, the predicted BER statistical results are slightly optimistic but are in good agreement. The short term (~ 1 minute) correlation coefficient between main beam and elevated beam signal powers was found to be negligibly small in both the predicted and measured results. The long term (~ months) correlation coefficient between the median RSL values was measured as 0.7. This value was used in a geometric model to estimate the long term correlation coefficient for other links using an exponential decrease in this coefficient with height differential between common volumes.

For the L-band predicted results, note that the angle diversity (2S/2A) system also outperforms the conventional frequency diversity (2S/2F) system. This result has not generally been anticipated due to larger squint losses (main beam RSL minus elevated beam RSL) in these lower frequency systems. The larger squint loss is due to wider antenna beamwidths which in turn result in greater separation between the common volumes. This greater separation leads to more decorrelation of the median RSL values in the angle diversity system and offsets this larger squint loss.

The effect of the long term decorrelation in median RSL values can be empirically evaluated from the C-band test link data by comparing angle and frequency diversity RSL distributions for the arithmetic mean of the receiver RSL values. Digital system performance is related to the geometric mean of the diversity branch signal-to-noise ratios or equivalently the arithmetic mean in dB. In the field tests, receivers 0, 1, 2, and 3 were main beam receivers and receivers 4, 5, 6, and 7 were elevated beam receivers. Two sets of angle diversity RSL data for 2S/2A configurations (Receivers 1,3,5,7 and

* square root of average of main beam and elevated beam variances

Receivers 0,2,4,6) can be compared with conventional 2S/2F (Receivers 0,1,2,3) RSL data. The arithmetic mean RSL distributions are plotted in Figure 12. The long term angle diversity improvement is seen to be about 3dB for both systems at 90% availability and about $1\frac{1}{2}$ and 4dB at 95% availability. These empirical results are consistent with a predicted improvement in yearly outage probability equivalent to 1.0 dB of greater median signal strength.

The measured distributions of the squint loss for the C-band system also illustrate the common volume decorrelation effect. These distributions are shown in Figure 13 for the 4 space/angle receiver pairs. A negative squint loss means that the elevated beam RSL is greater than the main beam RSL. With perfect correlation of median RSL values, these distributions would be horizontal lines.

Multipath delay spread and the delay between the main and elevated beam paths impact modem performance by the introduction of intersymbol interference. Figure 14 is typical of the distributions of the four receiver space/angle pairs. Median values of 2σ multipath spreads were 125 and 165 nanoseconds for the main and elevated beams, respectively. Multipath spreads as large as 300 ns were measured. The predicted values for this parameter were median 2σ values of 132 and 175 nanoseconds, respectively. The digital modem must also compensate for delay fluctuations between the main beam and elevated beam paths. In our digital tests we used a fixed delay compensation of 88 nanoseconds which was arrived at after a series of delay measurements using a RAKE receiver. This choice was appropriate as the long term data shows a delay variation over a 0 to 240 ns range. Under worst case conditions, the digital modem must compensate for 300 ns multipath spreads and a relative delay offset as much as 120 ns. With 4PSK modulation and a data rate of 6.3 Mb/s, the PSK symbol has a period of 317 nanoseconds. A three tap DFE modem [12] can generally accommodate 2σ delay variations up to twice the PSK symbol period with small degradation. Thus at a 6.3 Mb/s rate, these delay variations would not present a problem. However, at twice the data rate, 12.6 Mb/s, worst case conditions would result in significant performance degradations. This path because of its longer length is not typical of DCS C-band paths. However delay variations of this order or larger are predicted on L-band DCS paths. For the example L-band system used here the predicted median 2σ values are 131 and 279 ns for the main and elevated beams.

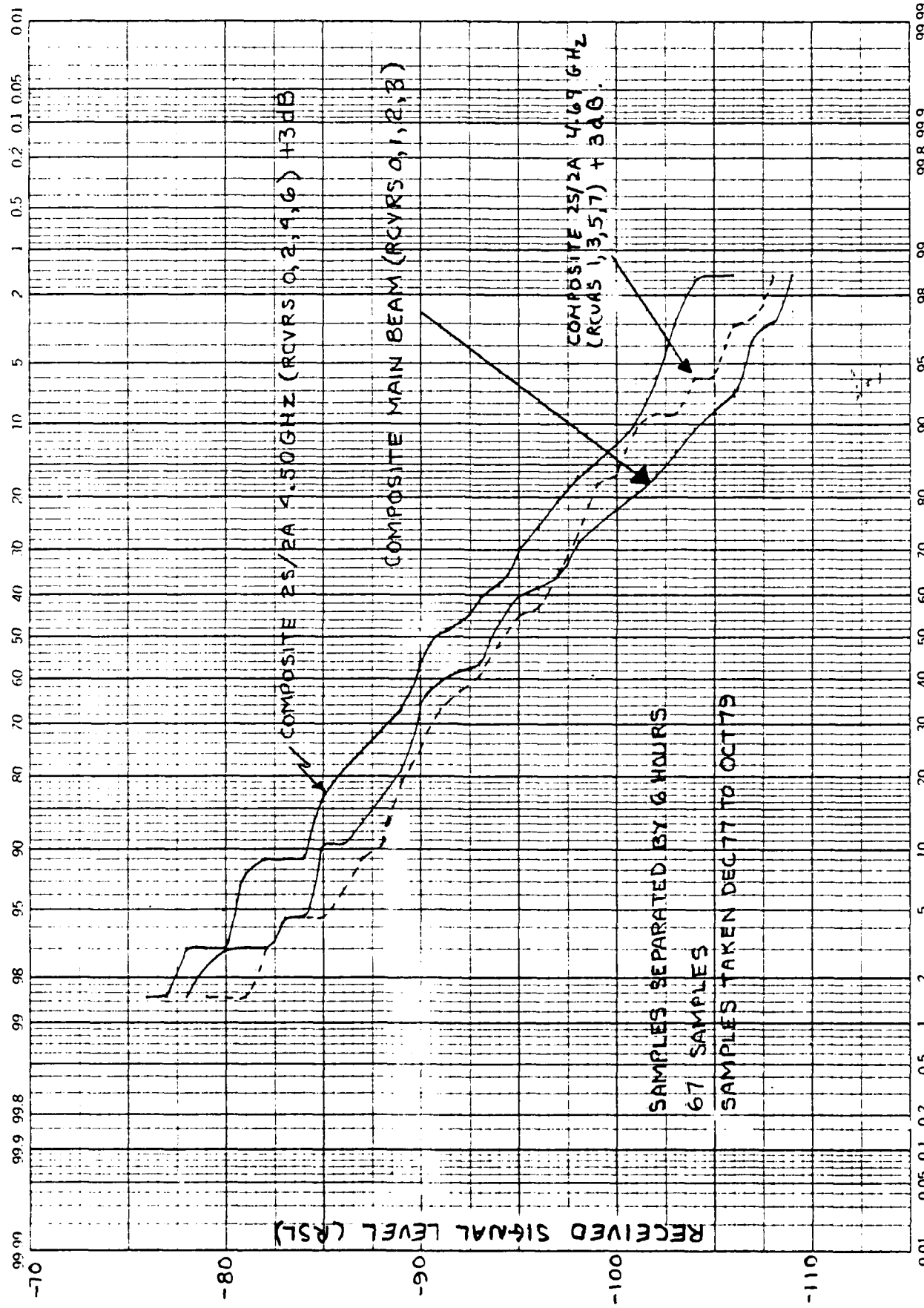


Fig. 12 Probability RSL Exceeds Ordinate

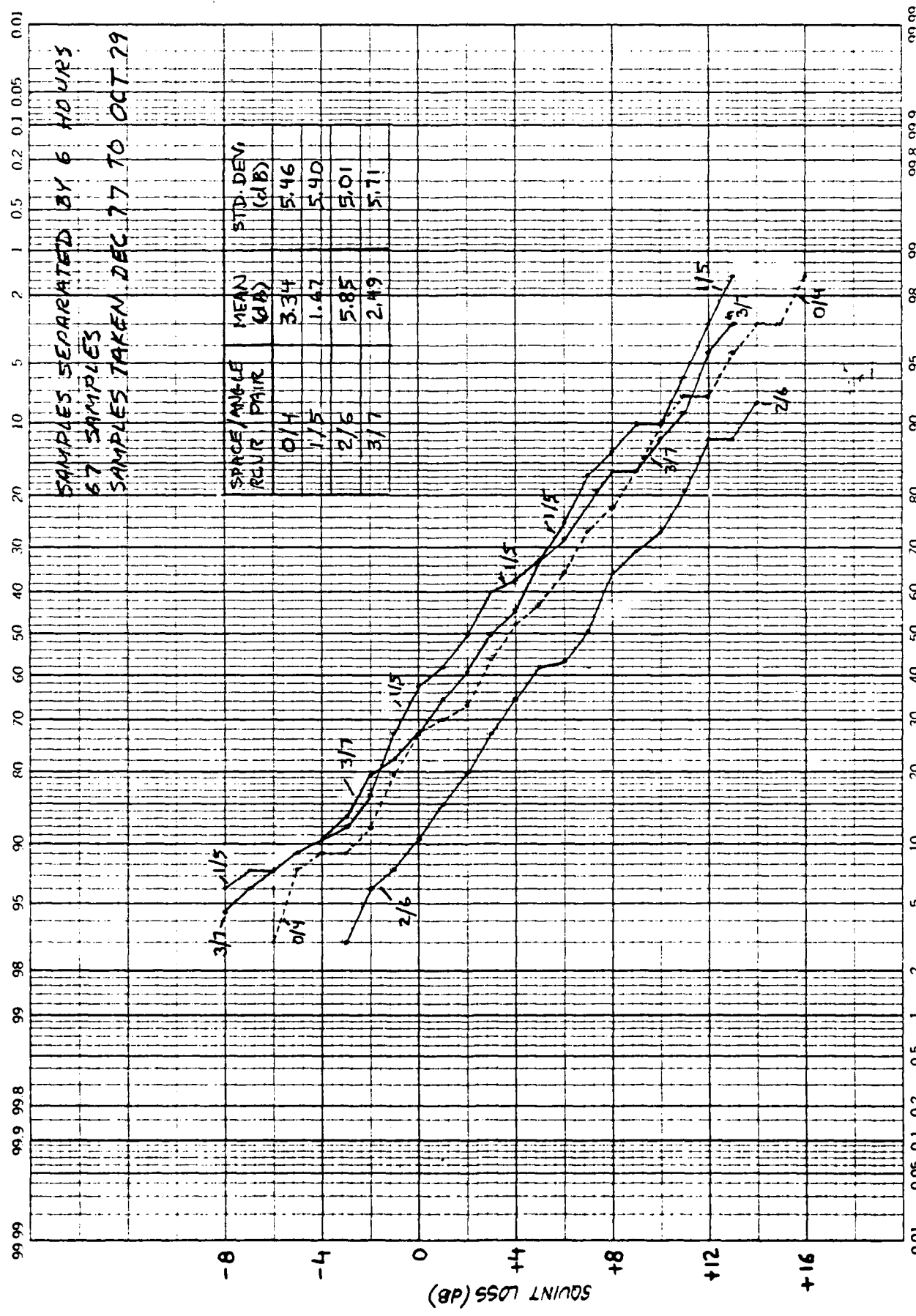
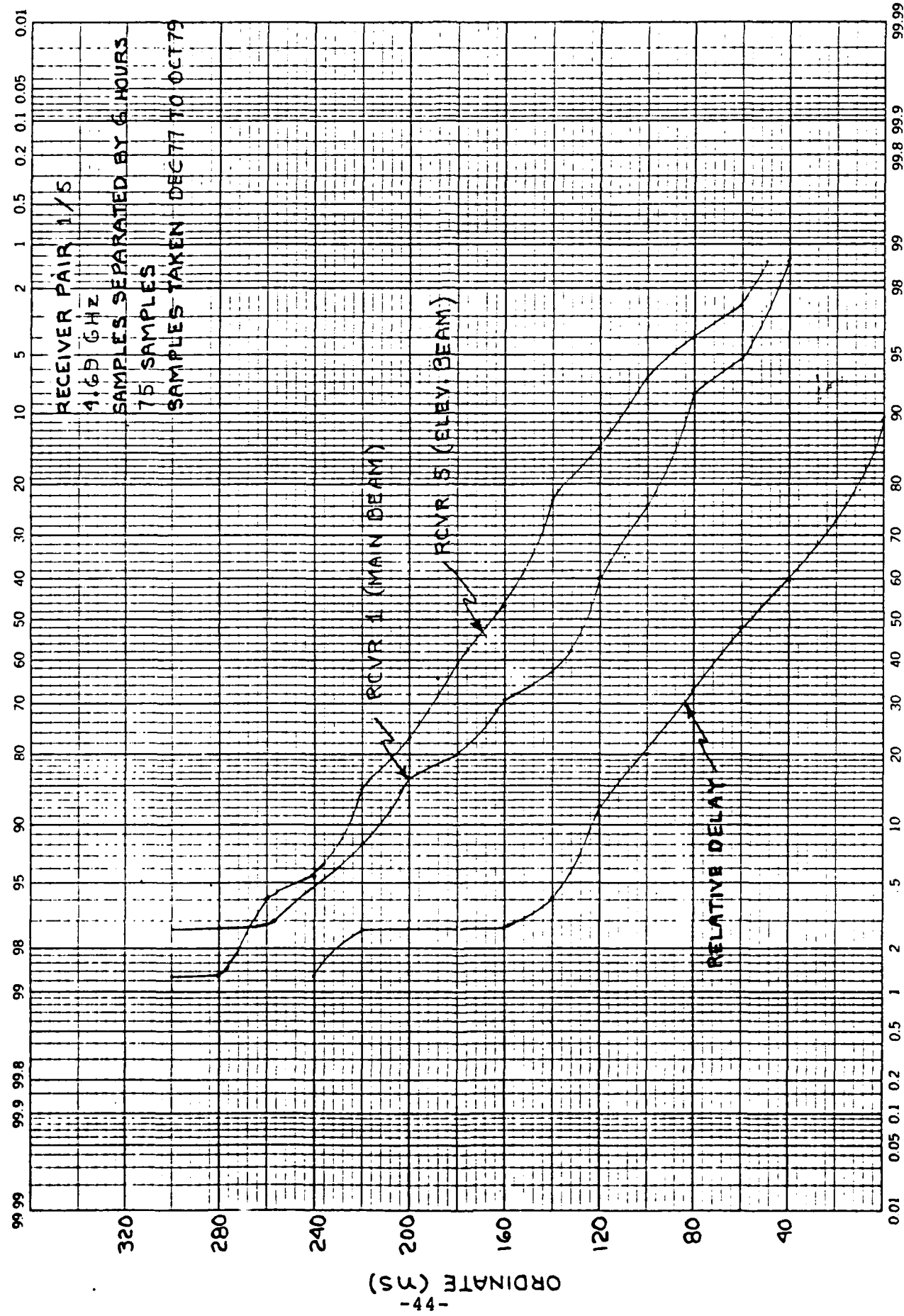


Figure 13 Squint Loss Distributions



PROBABILITY MULTIPATH SPREAD OR RELATIVE DELAY EXCEEDS ORDINATE
Figure 14 Multipath Spreads and Relative Delay, Space/Angle Pair 1/5

4.2 DIGITAL MODEM RESULTS

The MD-918 modem [11] is a quadruple diversity Decision-Feedback Equalizer with 3 taps in each of the four forward filter diversity branches and 3 taps in the backward filter for cancellation of intersymbol interference. Under this program a Pre-Detection Combiner (PDC) was developed to augment the MD-918 modem and thereby expand the modem receiver to eight forward filters. This expansion feature was required for tests of an eighth order 2S/2F/2A diversity configuration. The in-plant tests of the MD-918 and PDC were designed to verify the interoperation of these systems and to validate the modem prediction model described in Section 2.2. Interoperation was successful with a small degradation as the number of diversities was increased from 4 to 8. Good agreement between predicted and real time laboratory simulation results were obtained. These results were consistent with an earlier comparison of predicted and measured results reported on in [12].

The comparison between quad and eighth order diversity was accomplished simultaneously by using two receive modems and interconnecting the 8 receiver outputs in 2S/2F and 2S/2F/2A combinations. The results are shown in Figure 15 as average bit error rate vs. signal-to-noise ratio for the main beam diversity. These results correctly indicate the squint loss associated with the elevated beam. This squint loss plus the additional equipment combiner loss result in a rather small improvement for the increase in complexity (approximately 2 to 1 in the modem receiver) required. These tests suggest that the major advantage of angle diversity does not lie with augmenting frequency diversity but in replacing it. This result was anticipated by our prediction results and the field test emphasis was directed toward the following series of tests which compared 2S/2F and 2S/2A configurations.

Because the tests used transmission on two frequencies for the 2S/2F configuration, it was possible to evaluate two separate 2S/2A configurations, one at 4.5 GHz and one at 4.69 GHz. These tests were conducted during the winter when path loss and multipath spread conditions are at their worst. The results are shown in Figure 16 as average BER vs. main beam path loss. This comparison assumes two power amplifiers are used in any of the three configurations. The 4.5 GHz angle diversity system performed significantly better than the frequency diversity system for weaker signals suggesting considerable decorrelation between median main beam and elevated beam RSL values. The

AVERAGE BIT ERROR RATE

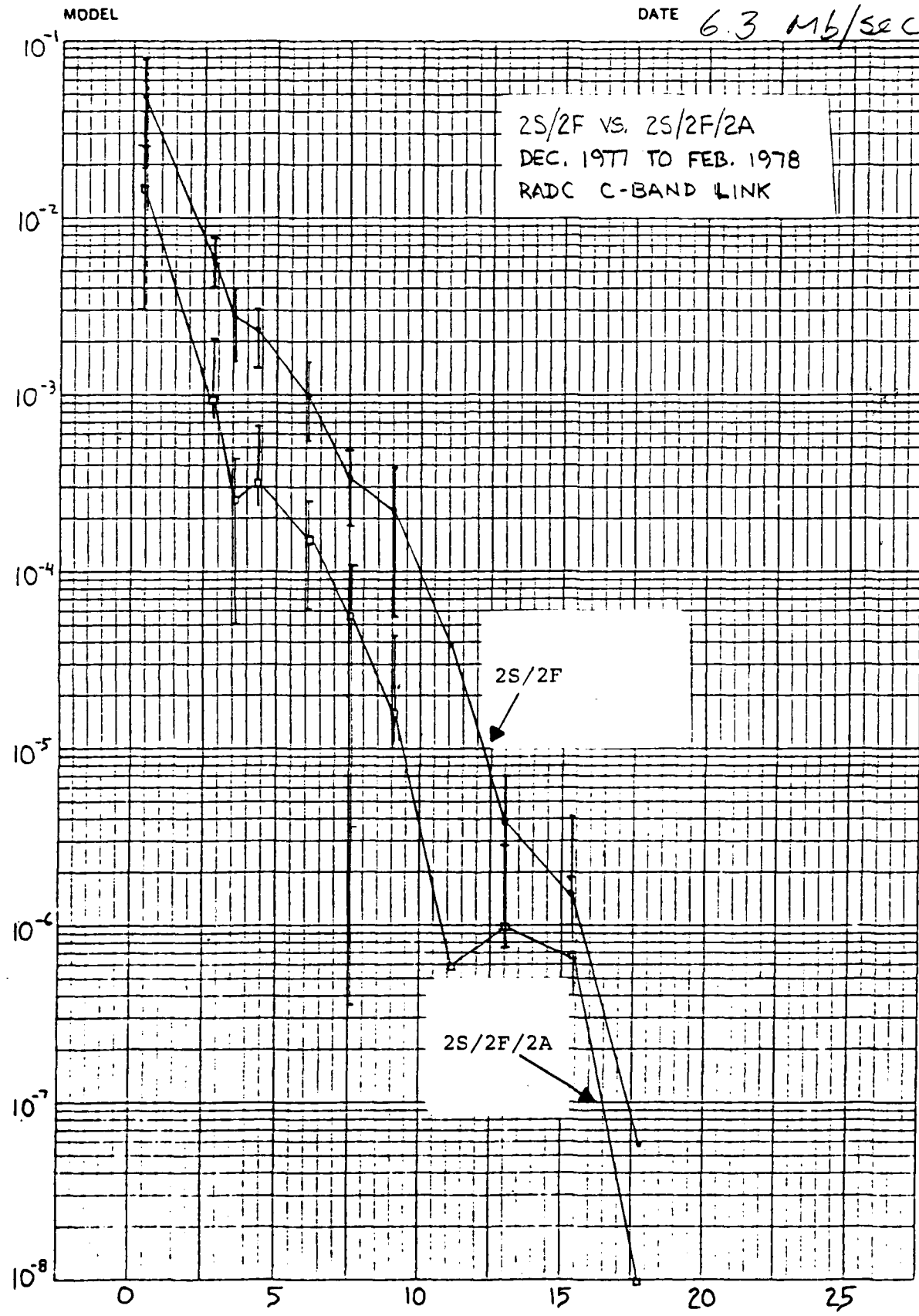


Figure 15 Average Bit Error Rate vs. Signal to Noise for Main Beam Diversity
 \bar{E}_b/N_0 PER MAIN BEAM DIVERSITY (dB)

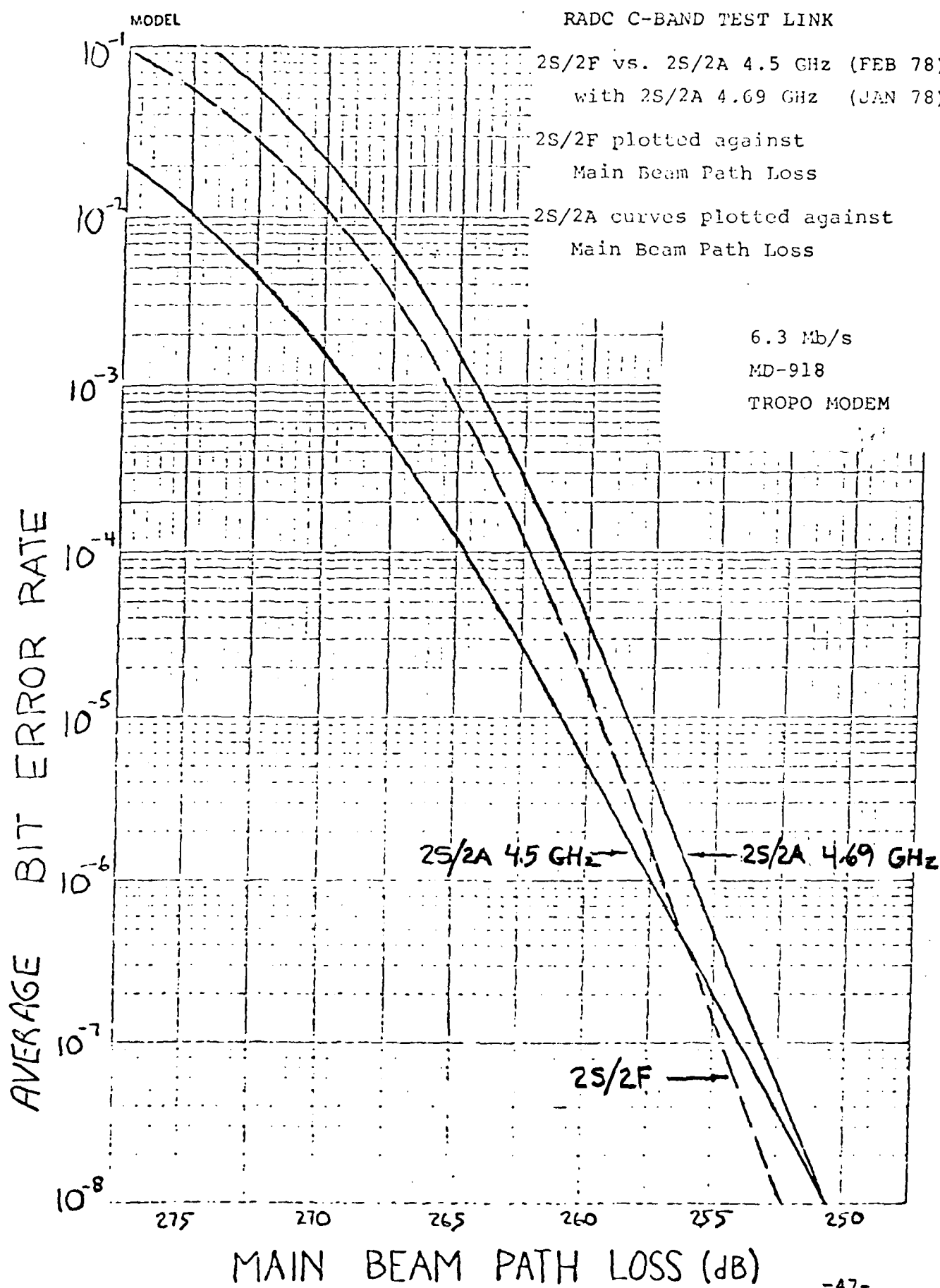


Figure 16 Quad Diversity Configurations Plotted Against Main Beam Path Loss

4.69 GHZ angle diversity system performed about 1dB poorer than the frequency diversity system. The poorer result may be attributed to RF receiver effects as the elevated beam receivers in this diversity configurations consistently were 1 to 2dB lower than the RF receivers for the elevated beam on the other frequency. The results of this simultaneous comparison therefore imply that angle diversity provides performance essentially equal or better than frequency diversity.

SECTION 5
CONCLUSIONS

The results from this investigation impact the development of future digital troposcatter systems in a number of ways. Because analog FM/FDM troposcatter systems generally require less bandwidth than digital, by almost a factor of two, the conversion to digital of 2S/2F systems requires twice as many bandwidth allocations. If, however, the digital conversion is accompanied by a conversion of the frequency diversity to angle diversity, the same or better diversity performance is realized but with the same total bandwidth requirements as the analog system rather than twice these requirements. In geographic areas such as Europe, where frequency assignments are hard to obtain, digital conversion may not be possible without use of angle diversity. The performance advantage of angle over frequency diversity has not been recognized in the past because of the emphasis on the squint loss and correlation of the elevated beam. Our results show that in wideband digital systems, short term correlation is not important and that the squint loss is compensated by both the second transmitter power amplifier which becomes available when a frequency to angle diversity conversion is made and a long term availability gain of angle diversity due to decorrelation in the two beams common volumes. Two power amplifiers are used in DCS communication applications to insure link reliability by providing redundancy.

The digital conversion of DCS troposcatter links will involve some links with carrier frequencies in the 4.4 to 5GHz band. The new prediction model developed under this program will be essential for determining upgrade recommendations and calculating network performance. The use of previous methods which were not derived for this frequency range may have led to unsatisfactory link service.

The small improvement resulting from extension of a 2S/2A system to a 2S/2F/2A eighth order diversity system is due to the 3dB penalty resulting from splitting the transmit power into two frequencies and combiner losses when eight signals are combined in one piece of equipment. Thus systems which do not meet outage rate standards generally require brute force dB improvement such as larger power amplifiers or antennas or coding application in lieu of frequency diversity. New work in the coding area shows significant improvements can be realized in high order diversity systems if coding is employed.

The absence of a correlation degradation in wideband digital angle diversity systems is due to the decorrelation effects of multipath on the two beams. Thus a correlation coefficient of 0.6 measured with CW signals which would degrade a narrowband digital system by 1dB has no significant effect on a wideband system. Thus in future design of angle diversity feedhorns every attempt should be made to reduce the beam separation and hence the squint loss. Reduction of the beam separation should not be at the expense of unacceptable coupling between horns, however.

The measured multipath spreads results which show an increase in 2σ by only about a factor of 1/3 are encouraging in that on most systems the present MD-918 DFE modem could accommodate the additional multipath spread associated with the elevated beam.

ACKNOWLEDGMENTS

Many people contributed to this overall effort. The authors would like to particularly note their appreciation for the equipment development efforts of Mr. P.F. Mahoney, Mr. G. Bonn of SIGNATRON, and Mr. J. Seavey, of Seavey Engineering; the test program and collection efforts of Mr. J. Eschle of SIGNATRON and the RADC personnel at Verona and Youngstown; the software contributions from Ms. L. Vears of SIGNATRON; and the contract guidance and support from Mr. G. Krause and his colleagues at Ft. Monmouth.

REFERENCES

- [1] A.B. Crawford, D.D. Hogg, and W.H. Kummer, "Studies in Tropospheric Propagation Beyond the Horizon", Bell Syst. Tech. J., Vol. 38, pp. 1067-1178, Sept. 1959.
- [2] J.H. Chisholm, L.P. Rainville, J.R. Roche, and H.G. Root, "Angular Diversity Reception at 2290MC Over a 188-Mile Path", IRE Trans. Commun. Syst., Vol. CS-7, pp. 195-201, Sept. 1959.
- [3] J.H. Vogelman, J.L. Ryerson, and M.H. Bickelhaupt, "Tropospheric Scatter System Using Angle Diversity", Proc. IRE, Vol. 47, pp. 688-696, May 1959.
- [4] D. Surenian, "Experimental Results of Angle Diversity System Tests", IEEE Trans. Commun. Technol., Vol COM-13, pp. 208-219, June 1965.
- [5] G.W. Travis, "Angle Diversity Tests", in Proc. Nat. Electron. Conf., Vol. 24, pp. 518-523, 1968.
- [6] P. Monsen, "Performance of an Experimental Angle-Diversity Troposcatter System", IEEE Trans. of Communications, Vol. COM-20, No. 2, April 1972.
- [7] V.N. Troitskiy, "Efficiency of Angle-Diversity Reception in Long-Distance Tropospheric Propagation", Telecommun. & Radio Eng., 1972, 27, pp. 17-23.
- [8] M.W. Gough, G.C. Rider, "Angle Diversity in Troposcatter Communications", Proc. IEE, Vol. 122, No. 7, pp. 713-719, July 1975.
- [9] T. Kono, T. Hirai, et al., "Antenna-Beam Deflection Loss and Signal Amplitude Correlation in Angle-Diversity Reception in UHF Beyond-Horizon Communication", J. Radio Rs. Lab., 1962, 9, pp. 21-49.
- [10] P. Monsen, High Speed Digital Communication Receiver, U.S. Patent No. 3, 879,664, April 22, 1975.
- [11] D.R. Kern and P. Monsen, Megabit Digital Troposcatter Subsystem, Final Report, ECOM-74-0040-F, April 1977.
- [12] P. Monsen, "Theoretical and Measured Performance of a DFE Modem on a Fading Multipath Channel", IEEE Trans. on Communications, Vol. COM-25, No. 10, pp. 1144-1152, October 1977.
- [13] P. Monsen, S. Parl, Adaptive Antenna Control (AAC) Program, Final Report, SIGNATRON, Inc., Lexington, MA, March 1980.
- [14] H.G. Booker, W.E. Gordon, "A Theory of Radio Scattering in the Troposphere", Proc. IRE, Vol. 38, pp. 401-402, 1950.

- [15] H.T. Friis, A.B. Crawford, D.C. Hoag, "A Reflection Theory for Propagation Beyond the Horizon", Bell System Tech. J., Vol. 36, pp. 627, (1957)
- [16] V.I. Tatarskii, The Effects of the Turbulent Atmosphere on Wave Propagation, Israel Program for Scientific Translation, Jerusalem, pp. 472, 1971.
- [17] F. Eklund, S. Wickerts, "Wavelength Dependence of Microwave Propagation Far Beyond the Radio Horizon", Radio Science, Vol. 3, pp. 1066-1074, 1968.
- [18] K.R. Hardy, I. Katz, "Probing the Clear Atmosphere with High Power, High Resolution Radars", Proc. IEEE, Vol. 57, pp. 468-480, 1969.
- [19] D.T. Gjessing, "Atmospheric Structure Deduced from Forward-scatter Wave Propagation Experiments", Radio Science, Vol. 4, pp. 1195-1210, 1969.
- [20] D.T. Gjessing, K.S. McCormick, "On the Prediction of the Characteristic Parameters of Long Distance Tropospheric Communication Links", IEEE Trans. Comm., Vol. COM-22, pp. 1325-1331, 1974.
- [21] P.L. Rice, A.G. Longley, K.A. Norton, A.P. Barsis, "Transmission Loss Prediction for Troposcatter Communications Circuits", NBS Tech. Note 101, 1965.
- [22] W.J. Hartman, R.E. Wilkerson, "Path Antenna Gain in an Exponential Atmosphere", J. Res. NBS, Vol. 63D, pp. 273-286, 1959.
- [23] L.P. Yeh, "Experimental Aperture-to-Medium Coupling Loss", Proc. IRE, Vol. 50, pp. 203, 1962.
- [24] R.E. Larsen, "A Comparison of Some Troposcatter Prediction Methods, IEE London Tropospheric Wave Propagation Conf., 1968.
- [25] P.F. Panter, Communication Systems Design: Line-of-Sight and Troposcatter System, McGraw Hill Book Co., New York, pp. 589, 1972.
- [26] D.L. Fried, "Optical Heterodyne Detection of an Atmospherically Distorted Wave Front", Proc. IEEE, Vol. 55, pp. 57-67, 1967.
- [27] E.E. Gossard, "Refractive Index Variance and its Height Distribution in Different Air Masses", Radio Sci., Vol. 12, pp. 89-105, 1957.
- [28] E. Brookner, "Improved Model for Structure Constant Variation with Altitude", Appl. Optics, Vol. 10, pp. 1960-1963, 1971.
- [29] M.D. Sirkis, "Contribution of Water Vapor to Index of Refraction Structure Parameter of Microwave Frequencies, IEEE Trans., Ant. Prop. AP-19, pp. 572-574, 1971.

- [30] S. Parl, "New Formulas for Tropospheric Scatter Path Loss", Radio Science, Vol. 14, No. 1, pp. 49-57, January-February 1979.
- [31] P. Monsen, "Performance of an Experimental Angle Diversity Troposcatter System", IEEE Trans. on Comm., Vol. COM-20, No. 2, pp. 242-247, April 1972.
- [32] V.N. Troitskiy, "Efficiency of Angle-Diversity Reception in Long-Distance Tropospheric Propagation", Telecommun. & Radio Eng., Vol. 27, pp. 17-23, 1972.
- [33] P. Monsen, S. Parl, "Assessment of Digital Tropo Transmission Using Angle Diversity", Report No. CSA-76-8085-5, October 1978, NATO RESTRICTED
- [34] J. Eschle, P. Monsen, "Adaptive Antenna Control (AAC) Program", Test Report No. CSA-76-8085-6, September 1980.
- [35] P. Monsen, S. Parl, J.N. Pierce, "Adaptive Antenna Control", Interim Technical Report, Contract No. DAAB07-76-C-8085, Prepared for US Army ECOM, Ft. Monmouth, NJ, December 22, 1976.

Distribution List - "Executive Summary, Adaptive Antenna Control (AAC) Program", report No. CSA-76-8085-8. (This distribution list covers the forty-five copies mentioned in the DD Form 1423 of the contract.)

Defense Technical Info. Ctr.
ATTN: DTIC-TCA
Cameron Station (Bldg. 5)
Alexandria, VA 22314
12 each copies

Code R123, Tech Library
DCA Defense Comm. Engr. Ctr.
1860 Wiehle Avenue
Reston, VA 22090
1 each copy

Defense Comm. Agency
Tech Library Ctr.
Code 205 (P.A. Tolovi)
Washington, DC 20305
1 each copy

Rome Air Development Ctr.
ATTN: Documents Library (TSLD)
Griffiss AFB, N.Y. 13441
1 each copy

Code R220
DCA Defense Comm. Engr. Ctr.
1860 Wiehle Avenue
Reston, VA 22090
4 each copies

Commander
U.S. Army Communications Systems Agency
ATTN: CCM-RD
Fort Monmouth, NJ 07703
11 each copies

Commander
U.S. Army Communications Command
ATTN: CL-OPS-SM
Fort Huachuca, AZ 85613
3 each copies

Commander
U.S. Army Communications-Electronics Command
ATTN: DRSEL-COM-RM-3
Fort Monmouth, NJ 07703
10 each copies

Commander
Rome Air Development Command
ATTN: RADC/DCCT
Griffiss Air Force Base, New York 13441
2 each copies